Fundamental Studies of Reactions between NO_3 Radicals and Organic Surfaces

Yafen Zhang

Thesis submitted to the faculty of the Virginia Polytechnic Institute and State University in partial fulfillment of the requirements for the degree of

MASTER OF SCIENCE
In
Chemistry

John R. Morris, Chair
Diego Troya
James M. Tanko
Brian M. Tissue

April 19th, 2012
Blacksburg, Virginia

Keywords: nitrate radicals, self-assembled monolayers, ultrahigh vacuum, electrophilic addition, hydrogen abstraction

Fundamental Studies of Reactions between NO_3 Radicals and Organic Surfaces

Yafen Zhang

ABSTRACT

Ultrahigh vacuum (UHV) surface science experiments were designed to study reaction kinetics and mechanisms of gas-phase NO_3 radicals with well-organized, highly characterized, organic thin films. The surface reactions were monitored *in situ* with reflection-absorption infrared spectroscopy (RAIRS). The oxidation states of surface-bound molecules were identified with X-ray photoelectron spectroscopy (XPS). Consumption of vinyl groups was observed concurrently with formation of organic nitrates in RAIRS. XPS spectra showed little oxidation of sulfur head groups. The observed rate constant was determined based on the consumption of carbon-carbon double bonds and the formation of organic nitrates. Using this rate constant, the initial reaction probability was determined to be $(3 \pm 1) \times 10^{-3}$. This reaction probability is approximately two orders of magnitude higher than that for the reactions between the same surface and pure O_3, which is due to the higher electron affinity of NO_3 relative to O_3. These results led to the development of a proposed mechanism that involves electrophilic addition of NO_3 to the double bonds. Reactions between NO_3 and a methyl-terminated SAM were also monitored *in situ* with RAIRS. In the CH_3-SAM studies, hydrogen abstraction was observed during NO_3 exposure. The results presented in this thesis should help develop an understanding of the fundamental interfacial reaction dynamics of NO_3 radicals with organic surfaces.

Acknowledgements

First and foremost, I would like to thank my mom and dad for their encouragement through my life. I would not be where I am today without their patience and guidance. Even though they are not with me now, they are always showing their support to pursue my dreams.

I would also like to give my sincere thanks to my advisor Dr. John Morris for being patient during my study at Virginia Tech. Dr. Morris has taught me, for example, how to improve my presentation and scientific writing, and most importantly, how to be an excellent scientist. His guidance and support are extremely appreciated.

Last, but certainly not least, I would like to thank the members of the Morris group who made the daily grind of graduate school enjoyable. In particular, I would like to acknowledge Jessica Lu, Erin Davis, Thomas Rockhold Jr., Alec Wagner, Amanda Wilmsmeyer, Dimitar Panayotov, Brandon Jeffery, Steve Burrows and Josh Abelard. During my time at Virginia Tech, I have made some of my best friends and I appreciate their encouragement and support, especially Xi Guo, Xiao Zhang, and Zhengmian Chang.

Table of Contents

List of Figures

List of Tables

Index of Acronyms

VOC	Volatile organic compounds
UV	Ultraviolet
FTIR	Fourier transform infrared
DES	Diethyl sebacate
SAMs	Self-assembled monolayers
UHV	Ultrahigh vacuum
XPS	X-ray photoelectron spectroscopy
RAIRS	Reflection-absorption infrared spectroscopy
MS	Mass spectroscopy
TDC	Thermal decomposition chamber
MCT	Mercury cadmium telluride
TPD	Temperature program desorption

Chapter 1

Introduction and Motivation

Thesis Statement

The objective of this research is to develop a fundamental understanding of the initial reaction kinetics and mechanisms in collisions of gas-phase NO_3 radicals with well-organized, highly characterized, organic thin films.

1.1 Aerosol Particles and Oxidative Gases in the Atmosphere

Aerosols are found throughout the atmosphere and significantly affect environmental processes, such as the absorption and scattering of light and cloud formation. In addition, the particulates can participate in heterogeneous reactions in the atmosphere.[1] Aerosols are defined as solid or liquid microscopic particles that range from 0.002 to 100 μm in size.[2] These particles can be formed through reactions of water vapor and other gases with SO_2 emissions from volcano eruptions or fossil fuel combustion.[3] Aerosols can also be generated directly from sources, such as smoke from forest fires, emissions of volatile organic compounds (VOCs) from industry, or vegetation.[4] The atmospheric particles also provide reactive surfaces for trace gases in the atmosphere, leading to chemical reactions that alter their size, chemical composition, and optical properties.[5,6] Changes in aerosol properties can further affect the scattering and absorption of light to alter the balance between incident and outgoing solar radiation. Changes in aerosol properties can also reduce the visibility in the atmosphere. Moreover, aerosols play an important role in cloud

formation, because they can act as cloud condensation nuclei (CCN).[7] Any change in the chemical or physical properties of aerosols can influence cloud droplet concentration and size distribution, and thus alter the solar radiation balance, impacting global climate.[2]

Ultraviolet (UV) light absorption by key inorganic gases in the atmosphere generates radicals, which drives important tropospheric chemistry. For example, photolysis of ozone produces molecular oxygen and atomic oxygen $O(^1D)$,[8] which can rapidly react with water vapor to form hydroxyl radicals. In addition, the reaction between O_3 and NO_2 leads to the formation of nitrate radicals, NO_3. Following absorption of visible light, NO_3 radicals thermally decompose to NO and NO_2 molecules. Subsequently, NO_2 can decompose to produce atomic oxygen $O(^3P)$ by photolysis.[9] Reactions between organics and NO_3 radicals produce organic nitrates and the hydroperoxyl radical (HO_2), which is the main source of the hydroxyl radical (OH) in the troposphere. Moreover, $O(^3P)$ produced by photolysis of NO_2 reacts with O_2 in the air to form ozone, as shown in Figure 1.1 below.

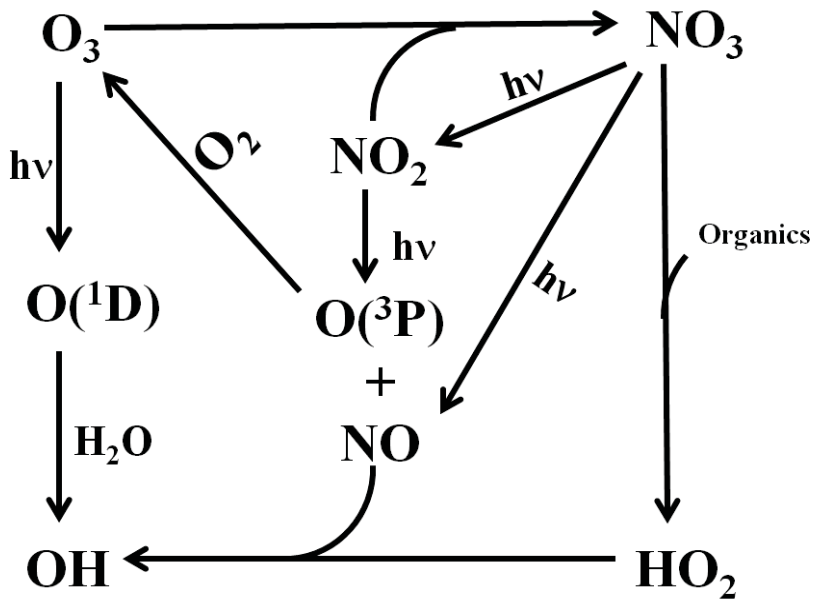

Figure 1.1. Cycling scheme of oxidative gases in the atmosphere.

The hydroxyl radical (OH) , the nitrate radical (NO_3), and ozone (O_3) are three important oxidative gases in the atmosphere, whose reactions with VOCs could form oxygenated products, such as carboxylic acid compounds and organic nitrates.[2] This process involves gas-to-particle transfer, which contributes to the formation of secondary organic aerosols.[1] While OH and O_3 make significant contribution to oxidation of atmospheric organics during the daytime, nitrate radicals act as the main initiator for oxidation of many organics at night. Table 1.1 shows the estimated lifetimes for the oxidation of some representative organic compounds by the three gases[2]. Here, it is apparent that OH has comparatively higher reaction rates than NO_3 or O_3. In addition, NO_3 radicals react much faster than ozone with these VOCs, even at lower concentrations. Although there are many studies that examine reactions between atmospheric organic compounds and OH or O_3,[1,10,11] there are far fewer studies into the chemistry of NO_3 radicals, particularly heterogeneous chemistry on

aerosol surfaces. Therefore, the focus of the work described in this thesis has been to perform fundamental research into the reaction of NO_3 radicals on well-organized organic surfaces. We aim to further understand reactions between organic aerosols and NO_3 radicals by studying the kinetics and mechanisms of interfacial reactions between NO_3 radicals and organic surfaces.

Table 1.1 Oxidative lifetimes of representative organics with corresponding atmospheric concentrations in unit of molecule cm^{-3} (adapted from Ref. 1).

Organic	OH (1×10^6)	O_3 (2×10^{12})	NO_3 (1×10^9)
n-Butane	5 days	≥ 1300 yr	205 days
trans-2-Butene	4.3 h	36 min	35 min
Toluene	2 days	≥ 400 days	138 days

1.2 Formation and Properties of Nitrate Radicals

Figure 1.2 shows the six resonance structures of the NO_3 radical. The unpaired electron on the oxygen atom makes it very reactive toward organics due to its ability of electrophilic addition to the carbon-carbon double bond or hydrogen abstraction from hydrocarbons.

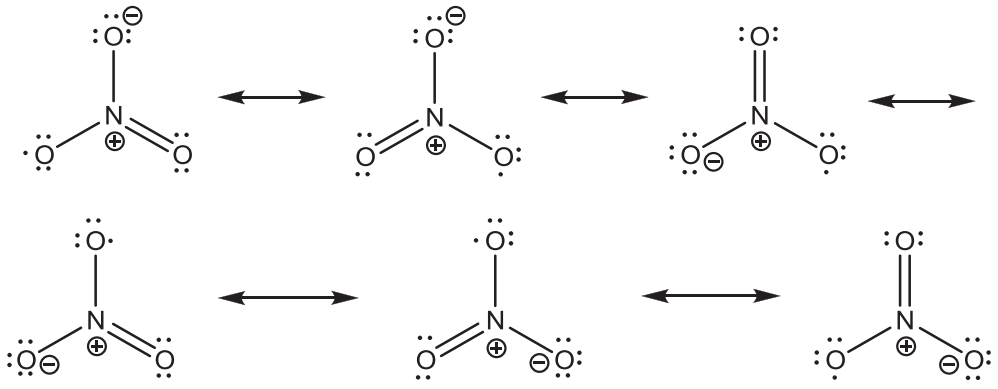

Figure 1.2. A schematic demonstrating the six resonance structures of NO_3.

The dominant source of nitrate radicals in the atmosphere is the reaction between NO_2 and ozone:[12,13]

$$2NO_2 + O_3 \longrightarrow N_2O_5 + O_2 \quad (1.1)$$

$$N_2O_5 \xrightarrow{\triangle} NO_3 + NO_2 \quad (1.2)$$

while, reaction (1.1) contributes to the formation of NO_3 radicals in the troposphere, nitrate radicals are rapidly consumed either by photolysis to $NO_2 + O$ or $NO + O_2$ during daylight hours,[12,14,15] or through gas-phase reaction with NO.[16]

$$NO_3 + NO \longrightarrow NO_2 + NO_2 \quad (1.3)$$

After sunset, a large decrease in the photolysis of NO_3 radicals results in the low concentration of NO that reduces the possibility of reaction (1.3).[17]

In addition to the above reactions, an important scavenging process for NO_3 involves the reaction with NO_2 to form N_2O_5:

$$NO_2 + NO_3 \leftrightarrow N_2O_5 \quad (1.4)$$

The temperature-dependent equilibrium constant K_{eq} for reaction (1.4) is calculated as below: [18,19]

$$K_{eq} = 2.7 \times 10^{-27} \times \exp(11000K/T)\ cm^3\ molecule^{-1} \quad (1.5)$$

$$K_{eq} = 2.90 \times 10^{-11}\ cm^3\ molecule^{-1} \text{ at } T=298\ K. \quad (1.6)$$

The equilibrium concentration of N_2O_5 is determined by the following equation:

$$[N_2O_5] = K_{eq} \times [NO_2] \times [NO_3] \quad (1.7)$$

According to this equilibrium expression, any depletion of N_2O_5 will affect the concentration of NO_3. In the atmosphere, N_2O_5 can react with water vapor (reaction (1.8)). Heterogeneous reactions between N_2O_5 and water in the aqueous layer of tropospheric aerosols or cloud particles produce nitric acid (reaction (1.9)).[18,19]

$$N_2O_5 + H_2O \longrightarrow 2HNO_3 \quad (1.8)$$

$$N_2O_5 + (H_2O)_{eq} \longrightarrow 2(HNO_3)_{eq} \quad (1.9)$$

In addition to the loss of NO_3 in the atmospheric reactions shown above, NO_3 can be scavenged by VOCs. The reaction between NO_3 radicals and selected VOCs will be discussed in the next section.

1.3 Gas-phase Reactions of Nitrate Radicals (NO_3) with Unsaturated and Saturated Hydrocarbons

Since Noxon et al.[20] first reported the presence of NO_3 radicals in the troposphere ($\leq$ 10-15 km), there have been several studies that have examined the reactions between NO_3 radicals and volatile organic compounds.[18,21] It is now well known that the nitrate radical is a strong oxider that initiates nighttime degradation of environmental organic compounds, such as isoprene, monoterpenes, aromatic hydrocarbons,[22,23] to form peroxyl radicals.[24]

Organic compounds from biogenic sources react with NO_3 radicals in the atmosphere. Biogenic hydrocarbons, such as isoprene and the monoterpenes that are emitted from vegetation and other natural sources, contribute significantly to global air pollution.[23,25] In Rasmussen's chamber studies,[26] they estimated global forest hydrocarbon emissions to be 1.75×10^8 metric tons per year. A large quantity of biogenic organic compounds is removed by nighttime reactions with NO_3. Winer and co-workers[23] compared organic lifetimes acquired from reactions of isoprene and several monoterpenes with NO_3 to their reactions with ozone and OH, both in "clean"

atmosphere (defined as 30 ppb of O_3, 0.04 ppt of OH during daytime, and 10 ppt of NO_3 during nighttime), and "moderately" polluted atmospheres (defined as 200 ppb of O_3, 0.16 ppt of OH during daytime, and 100 ppt of NO_3 during nighttime). From Table 1.2, it is apparent that the reaction of NO_3 with the four compounds results in much shorter organic lifetimes, due to much higher reaction rates, than with OH and O_3, especially in the "moderately" polluted atmosphere at night. Reactions between the unsaturated hydrocarbons and NO_3 radicals are proposed to be initiated by electrophilic addition of NO_3 to the carbon-carbon double bond.

Table 1.2 Calculated lifetimes of isoprene and three monoterpenes from their reactions with ozone, OH and NO_3 radicals (adapted from Ref. 23).

Compounds	Organic lifetime					
	"Clean" atmosphere			"Moderately polluted" atmosphere		
	$\tau(O_3)$	τ(OH)/h	$\tau(NO_3)$/min	$\tau(O_3)$	τ(OH)/min	$\tau(NO_3)$/min
Isoprene	32 h	2.9	216	10 h	44	22
α-Pinene	4.6 h	4.6	20	1.4 h	72	2
β-Pinene	18 h	3.6	50	5.5 h	54	5
d-Limonene	36 min	2.0	9	11 min	30	0.9

As mentioned above, the nitrate radical reacts with unsaturated groups through electrophilic addition to the carbon-carbon double bonds, which leads to the formation of an alkyl radical adduct intermediate ①(Figure 1.3). The radical intermediate either collisionally stabilizes ②or decomposes to an oxirane ③by breaking the weaker CO-NO_2 bond.[27] In the presence of oxygen, the collisionally stabilized radical may be

further oxidized to form a nitroxy peroxyl radical ④. The nitroxy perxyl radical then reacts with NO_2 to produce a thermally unstable peroxydinitrate ⑤. This peroxydinitrate can then form the alkoxyl radical ⑥through self reactions. Finally, the alkoxy radical either further reacts with NO_2 to produce dinitrates ⑦, or decomposes to carbonyl compounds.[2] The reaction pathways are shown in Figure 1.3.

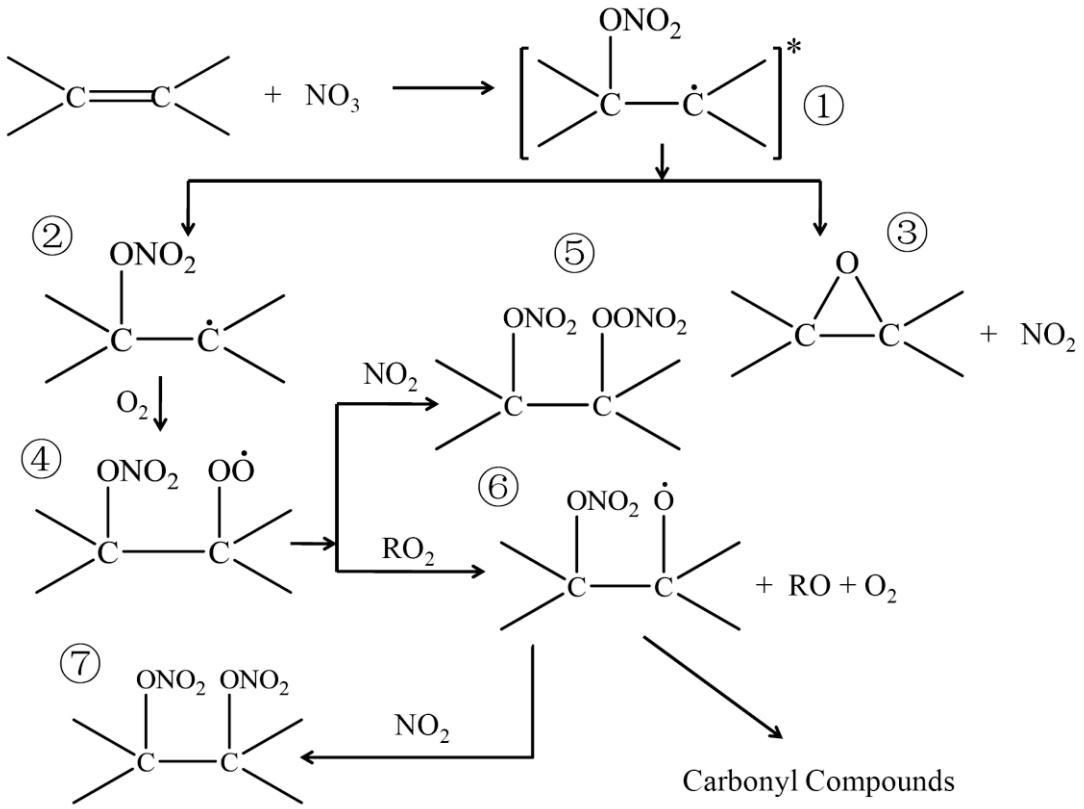

Figure 1.3. A schematic of the mechanism for reactions between NO_3 and alkenes.

In addition to electrophilic addition of NO_3 to the carbon-carbon double bond, NO_3 can also react with saturated hydrocarbons. In a process similar to OH, NO_3 can abstract hydrogen atoms from alkanes, to produce nitric acid and alkyl radicals, which are then oxidized by O_2 to form alkylperoxyl radicals, RO_2. The reactions are shown in Equation (1.10) and Equation (1.11) and the corresponding rate constants are ~ 10^{-11} cm^3 $molecule^{-1}$ s^{-1}.[2] Peroxyl radicals can undergo self-reacting, which is one

source of peroxides in the atmosphere (reaction (1.12)).[24] In addition, the peroxyl radical RO_2 can be further oxidized by NO_3 to form the RO product (reaction (1.13)), which complements the conversion of RO_2 to RO during the daytime.[2,28] The conversion is important because it leads to the formation of HO_2 radicals (reaction (1.14)), and thus to the generation of peroxides or OH radicals in the dark (reaction (1.15)).[29]

$$NO_3 + RH \longrightarrow HNO_3 + R \quad (1.10)$$

$$R + O_2 \longrightarrow RO_2 \quad (1.11)$$

$$CH_3O_2 + CH_3O_2 \longrightarrow CH_3OOCH_3 + O_2 \quad (1.12)$$

$$CH_3O_2 + NO_3 \longrightarrow CH_3O + NO_2 + O_2 \quad (1.13)$$

$$CH_3O + O_2 \longrightarrow HO_2 + CH_2O \quad (1.14)$$

$$HO_2 + NO_3 \longrightarrow OH + NO_2 + O_2 \quad (1.15)$$

The generated alkylperoxyl radicals can also react with atmospheric NO, NO_2, HO_2, or even another RO_2, through processes with rate constants on the order of ~ 10^{-12} cm^3 $molecule^{-1}$ s^{-1}.[24,30,31] One other possible reaction channel after generation of alkylperoxyl radicals is through decomposition of the excited RO_2^* intermediate before it is stabilized. This decomposition leads to the formation of an alkene and HO_2. However, the probability of this process is so small that only about 1% or lower percentage of the excited RO_2^* is involved.[32] The initial H-abstraction step is much slower than reactions involving the radical products (k = ~10^{-18}-10^{-16} cm^3 $molecule^{-1}$ s^{-1}). These reaction rates are about 3-5 orders of magnitude lower than rates for reactions between NO_3 and alkenes, which makes reactions between NO_3 and alkanes negligible in the presence of alkenes.[31]

Because the nitrate radical is a major scavenger of organic compounds in the atmosphere, researchers have explored gas-phase reactions of NO_3 with unsaturated and saturated hydrocarbons, especially alkenes and alkanes. These reactions are always initiated by either addition of NO_3 to the carbon-carbon double bond or hydrogen abstraction from hydrocarbons, which leads to the formation of nitric acid, organic nitrates and other products.[33] Therefore, investigations on the reaction kinetics have drawn scientists' attention for further exploration on the reaction mechanism.

Studies of NO_3 chemistry by Atkinson et al. first used two methods to determine rate constants at room temperature for reactions of NO_3 with the following organics: ethane $(6.1 \pm 2.6) \times 10^{-17}$, propene $(4.2 \pm 0.9) \times 10^{-15}$, trans-2-butene $(2.11 \pm 0.24) \times 10^{-13}$, m-xylene $(7.6 \pm 3.5) \times 10^{-17}$, all in units of cm^3 $molecule^{-1}$ s^{-1}.[34] Because the decomposition of N_2O_5 produces NO_3 radicals which are very reactive to all organics, it was difficult to study the reaction kinetics by measuring the decay of NO_3 directly. Based upon the assumption that only NO_3 radicals react with the organics, a method that monitored N_2O_5 decay with the [organic]/[NO_2] ratio was used. By plotting dln [N_2O_5]/dt + k_1 versus [organic]/[NO_2], the rate constant k_2 for reactions between NO_3 and the organic was determined from the corresponding slope, as shown in Equation (1.16),[34]

$$-K(\mathrm{dln}\,[N_2O_5]/dt + k_1) = k_2[\mathrm{organic}]/[NO_2] \qquad (1.16)$$

where K is the equilibrium constant for the inverse of reaction (1.4), k_1 is the rate constant for loss of N_2O_5, and k_2 is the rate constant for reactions of NO_3 with the organic.

The observations that the N_2O_5 decay rate increased linearly with the [organic]/[NO_2] ratio and not with [organic] confirmed the assumption that the NO_3 radical, and not N_2O_5, was actually the reactive species. However, intermediates formed from reactions of NO_3 with the experimental organics could lead to secondary reactions that also caused the consumption of N_2O_5, which would increase the N_2O_5 decay rate. The increase in the N_2O_5 decay rate could result in a higher measured rate constant than the true rate constant for reactions of NO_3 with the experimental organic reactant. Therefore, the other method, which utilized the relative rate technique by plotting ln ([organic]$_{t0}$/[organic]$_t$) – D_t against ln ([reference organic]$_{t0}$/[reference organic]$_t$) – D_t, was applied to determine the rate constants. The relationship also yielded a straight line with a slope equal to the rate constant, as shown in Equation (1.17),[34]

$$\ln([\text{organic}]_{t0}/[\text{organic}]_t) - D_t = (k_3/k_4)[\ln([\text{reference organic}]_{t0}/[\text{reference organic}]_t) - D_t] \quad (1.17)$$

where k_3 is the rate constant for reactions between NO_3 and the organic and k_4 is the rate constant for reactions between NO_3 and the reference organic, and D_t is the dilution factor at time t, caused by N_2O_5 additions.

Since the results obtained by the relative rate technique showed an increased sensitivity, this more accurate method has been used in most kinetic studies[35-37] of gas-phase reactions between NO_3 and atmospheric hydrocarbons.

Aschmann et al. used the same relative rate technique to study the kinetics for reactions of NO_3 radicals with a series of linear and branched C_5-C_7 1-alkenes to

explore inductive and steric effects of alkene reactions.[35] They found that the reaction rate increased with an increasing number of carbons adjacent to the double bond. For a given carbon number, by assuming that the inductive effect was independent of the degree of branching, the steric effect of methyl and dimethyl substituted alkenes was the primary cause for any differences in the rate constant, which were expected to decrease in the following order (for methyl/dimethyl substitution of 1-pentenes): 4- < 4,4- < 3,4- < 3,3-. Therefore, the conclusion made from the steric effect study was consistent with the proposed mechanism for reactions of NO_3 with alkenes. The mechanism states that the reaction is initiated by an electrophilic addition of NO_3 to the double bond.

Recently, researchers have studied the reaction kinetics of NO_3 with a variety of other organic compounds found in the atmosphere, such as: methacrylates, which are widely used in polymer production; 3-methylfuran, which is released into the air during fossil fuel combustion; and thymidines, a DNA nucleoside. Salgado et al.[36] explored the kinetics and possible products for reactions between NO_3 and methacrylates. The rate coefficients for reactions between NO_3 and different chain-length methacrylates were on the order of 10^{-15} cm^3 $molecule^{-1}$ s^{-1}. Fourier Transform Infrared Spectroscopy (FTIR) was used to identify products. Characteristic peaks for nitroperoxy compounds ($OONO_2$), nitrooxy compounds (ONO_2) and carbonyl compounds were assigned. The first step for reactions of NO_3 with different chain-length methacrylates was proposed to be an electrophilic addition to the double bond. This conclusion was made based on the observation that the rate coefficient

increased with the increasing substitution at the C=C group. Later, Tapia et al.[38] investigated atmospheric degradation of 3-methylfuran by using FTIR and observed evidence for the creation of nitroperoxy compounds, nitrooxy compounds, and carbonyl compounds. In addition, they identified epoxy compounds that degraded with time, indicating that these products were thermally unstable after formation. Their results agreed with the mechanism that the reaction is initiated by an addition of NO_3 to the double bond and that the addition likely takes place at the position where the most stable intermediates are generated. Interestingly, Wille et al.[39] proposed a third pathway for the initiation of NO_3 reactions with organics. Their mechanism suggests that NO_3 reacts through electron transfer, rather than H-atom abstraction or electrophilic addition to double bonds. However, this electron transfer mechanism has not been confirmed through additional studies.

1.4 Heterogeneous Reactions of NO_3 with Organic Surfaces

Aerosols provide reactive surfaces to oxidative gases in the troposphere. Many important heterogeneous processes proceed through reactions between oxidizing gases, such as NO_3, and surface adsorbed reactants.[40]Although gas-phase reactions of NO_3 with organics have been widely strudied[34,35,37-39], there remains few fundamental studies into the reactions between NO_3 and organic surfaces.

Xiao et al. investigated the reactive uptake of NO_3 on binary mixtures containing an unsaturated organic compound and saturated molecules, which were designated matrix molecules.[41] The loss of oxidative gases during reactions is generally described

by uptake coefficient (γ), defined as the ratio of the number of molecules lost to the surface to the number of molecules that collide with the surface, as shown in Equation (1.18).[42]

$$\gamma = \text{number of molecules lost/number of colliding molecules} \quad (1.18)$$

Under the experimental conditions, reactions of NO_3 on solid-liquid mixtures were performed, i. e. mixtures partially composed of diethyl sebacate (DES) and a liquid mixture of methyl oleate and DES. Their NO_3 experiments on binary liquid mixtures showed that, even with a small amount (about 2.3%) of methyl oleate added to the pure matrix, the reactive uptake coefficient increased by a factor of 20 compared to the pure case. The measured uptake coefficient decreased after a period of NO_3 exposure, because only the top few monolayers in the exposed liquid were reactive; once the double bonds were oxidized, the reactivity decreased rapidly. These results showed that surface reaction lifetimes were shorter than bulk reaction lifetimes, probably due to more surface reaction sites.

Both bulk and surface reaction mechanisms were proposed in their work, but due to the lack of a well-defined surface, neither can be certainly concluded. Therefore, Gross et al.[43] employed self-assembled monolayers (SAMs) to explore the products and kinetics for NO_3 collisions with well characterized organic surfaces. Self-assembled monolayers of alkanethiols or alkenethiols on gold, which are easily prepared and form strong adsorbate-substrate bonds provide control over the surface order, orientation, and terminal functional group. The experimental uptake coefficient for NO_3 on alkene SAMs was higher than the values obtained using liquid or solid

films,[44] due to the exposed double bonds at the interface rather than buried in the bulk. In their infrared spectroscopic and x-ray photoelectron spectroscopic measurements, several expected products, reported in previous gas-phase studies, were not observed, likely due to the loss of the species during sample transfer between instruments. The difficulty in identifying reaction products required *in situ* measurements of the surface reaction.

As a result, more work exploring gas-organic surface reactions with NO_3 is needed to give researchers insight into the kinetic and mechanic details of these important atmospheric interactions. In addition, almost all investigations of nitrate radical reactions with organic surfaces to date have been performed on poorly characterized surfaces under ambient conditions. Therefore, there remain many fundamental aspects of the interfacial chemistry that have yet to be explored.

1.5 Summary and Research Objectives

Reactions between NO_3 radicals and organic surfaces contribute to the change in physical or chemical properties of organics-coated aerosols, which can alter the solar radiation balance, and thus affect global climate. However, the exact products and the mechanism for those reactions are not thoroughly understood and need further exploration.

Therefore, the research in this thesis is to focus on the fundamental study of the kinetics, products, and mechanisms for reactions of NO_3 radicals with organic surfaces to better understand the fate, lifetime and environmental impact of organic

aerosols in the atmosphere. The reactions between NO_3 and methyl/vinyl terminated SAMs are targeted. The chemical reactions are isolated from interfering reactions of background gases by incorporating ultrahigh vacuum system (UHV). This UHV system allows us to perform the surface exposure with controlled amounts of NO_3 through a dosing device. *In situ* reflection-absorption infrared spectroscopy (RAIRS) is used to identify the surface-bound products and study the reaction kinetics. The organic surfaces will be analyzed before and after the NO_3 exposure by x-ray photoelectric spectroscopy (XPS) to probe the oxidation states of surface-bound species. These studies will provide the rate constants and reaction probabilities that are useful to explore the reaction mechanism.

Our overall objectives are to study the fundamental chemistry of NO_3 reactions on organic surfaces to help better predict the environmental fate of nitrate radicals and organic materials. The goals will be achieved through the pursuit of three key experimental objectives:

1. Measure the initial reaction probability for NO_3 collisions with a vinyl-terminated self-assembled monolayer;

2. Determine the reaction kinetics and mechanisms of NO_3 with the well-ordered vinyl-terminated SAM;

3. Develop an understanding for how the interfacial reactions of NO_3 with SAMs depend on the chemical functionality of the organic materials.

Chapter 2

Experimental Approach

2.1 Introduction

Atmospheric aerosols significantly affect environmental processes, such as the absorption and scattering of light and cloud formation. These particles can provide organic surfaces to oxidative gases in the atmosphere. Reactions between the organic surfaces and atmospheric oxiders, such as nitrate radicals (NO_3), can alter the chemical or physical properties of organic aerosols. These changes will affect the solar radiation balance and global climate. In the past, scientists mainly investigated nitrate radical reactions with organic surfaces that were performed on poorly characterized surfaces under ambient conditions.[34,43] Therefore, many fundamental aspects of the interfacial reaction between NO_3 and organic surfaces need to be explored.

My research goal is to develop a fundamental understanding of the reaction kinetics and mechanism of NO_3 radicals with highly characterized organic surfaces. An ultrahigh vacuum (UHV) system was used for this purpose. In the UHV system, background gases have been eliminated to control the type of molecules that interact with the organic surface. The reactions between NO_3 and the organic surface were monitored *in situ* with Reflection-Absorption Infrared Spectroscopy (RAIRS). X-ray Photoelectron Spectroscopy (XPS) was used to analyze the surface before and after NO_3 exposure. In addition, desorbed products can be detected in the mass spectrometer.

2.2 Ultrahigh Vacuum System

To study the kinetics of reactions that occur at the gas-surface interface, it is important to perform the experiments under well-defined conditions.[45] The XPS and MS used in this work rely on the detection of electrons or ions. Therefore, the mean free path of these particles must be much greater than the dimensions of the system, such that the particles travel directly to the detector without being interrupted by the surrounding gas molecules. The mean free path in an ultrahigh vacuum system of 10^{-9} torr is 5×10^{5} m, which is more than sufficient for performing XPS. In addition to a large mean free path, ultrahigh vacuum is required in order to begin experiments with a clean surface and ensure that the surface does not become contaminated by background gases.[46] By assuming a unit sticking probability, the minimum time for a clean surface to be covered by a monolayer of adsorbates is $\sim 10^{-9}$ s at the atmospheric pressure and $\sim 10^{3}$ s at a pressure of 10^{-9} torr.[46] Therefore, the UHV system allows us to reduce contributions to the surface chemistry from background gases, such as H_2O and O_2, and isolate reactions to those between NO_3 radicals and the surface.

In this work, the UHV experiments were designed to study the kinetics and mechanism of reactions between nitrate radicals and organic surfaces. RAIRS, XPS and Mass Spectroscopy (MS) are attached to the chamber to perform surface analysis before, during and after exposing the surface to the reactive gas. A schematic of the instrument is shown in Figure 2.1.

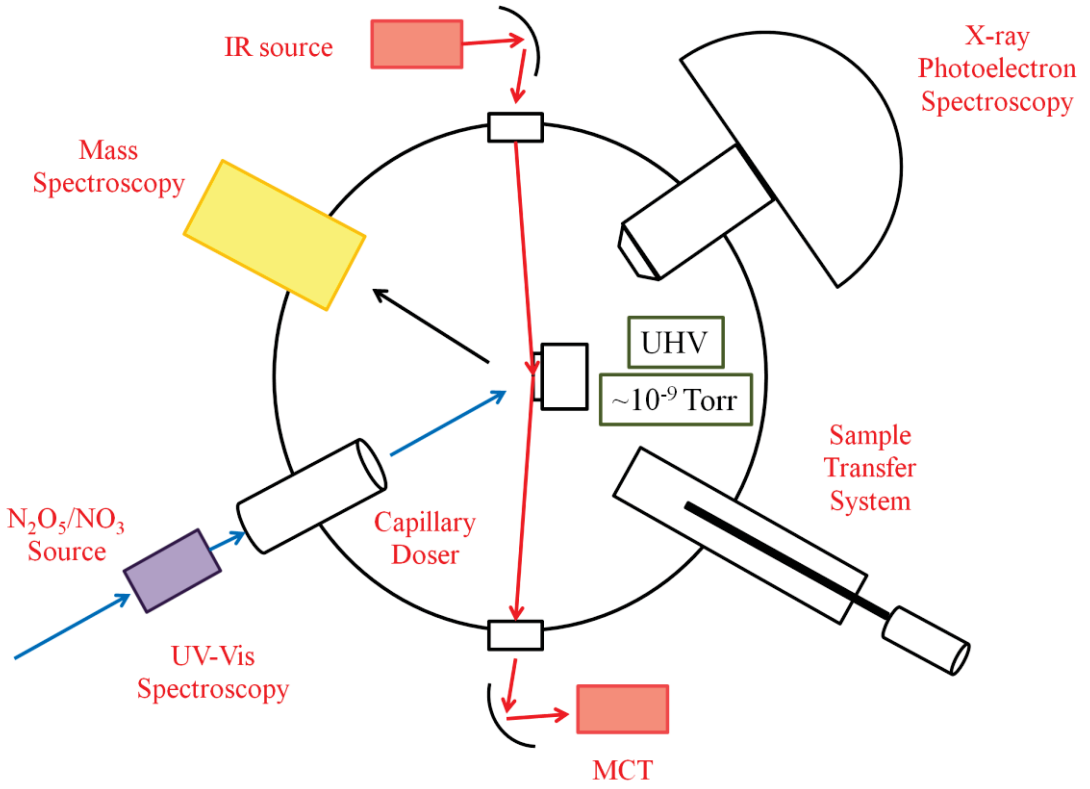

Figure 2.1. A scheme of the experimental setup.

2.3 Nitrate Radical Generation, Storage, and the Exposure Experiment

Figure 2.2 shows a schematic representing the various components of the nitrate radical synthesis and storage system. Production of NO_3 began by first closing the valves. Next, the system was purged with ultrahigh pure nitrogen (Airgas Specialty Gases) through valves 2, 3, 4, 6, and 7. Then, the system was evacuated by a diaphragm pump (Pfeiffer Vacuum). After this evacuation, valve 7 was closed to isolate the system. Valves 2 and 3 were closed and valves 1 and 7 were opened to flow research grade oxygen (Airgas Specialty Gases) through the system. Then, the ozone generator (RMU16-DG3 Ozone Generator Frame System) was turned on and valve 5 was opened to introduce NO (Sigma-Aldrich, Inc). Oxidation of NO to NO_2 by O_3 occurred as the gases combined in the mixing vessel. After this oxidation, NO_2 reacted with excess O_3 to form N_2O_5 (reaction (2.1)):

$$2NO_2 + O_3 \longrightarrow N_2O_5 + O_2 \quad (2.1)$$

which was trapped into the Pyrex glass trap vessel that was cooled in a dry ice-ethanol bath. After trapping N_2O_5 for about 2 hours, the ozone generator was turned off and the N_2O_5 trap was isolated from the system. Finally, excess O_3 was pumped away.

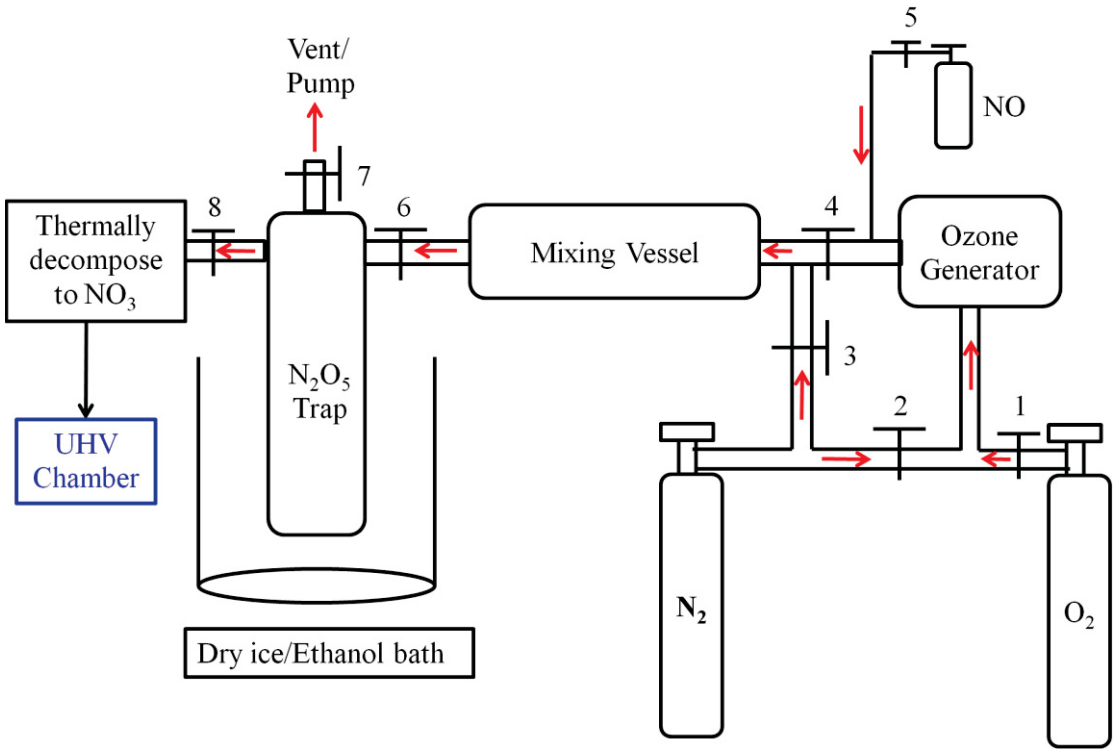

Figure 2.2. NO_3 generation and storage system. The labeled components are: (1-5) needle valves, (6-8) Teflon-sealed glass valves.

To perform the exposure experiments, the N_2O_5 trap was slowly warmed and introduced into a heating jacket. The pressure of the N_2O_5 gas was measured by a baratron gauge (MKS Instrument, Inc). A K-type thermocouple, which was placed in the heating tape, was used to monitor the temperature. N_2O_5 molecules were thermally decomposed to NO_3 radicals at ~324 K in the Thermal Decomposition Chamber (TDC). The NO_3 radicals were then dosed into the UHV chamber through a capillary array doser, as shown in Figure 2.3.

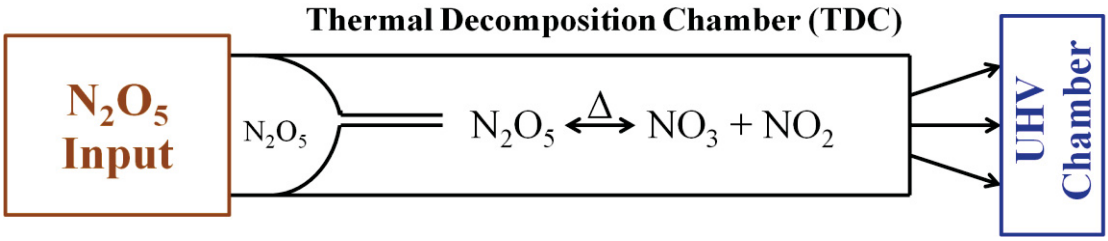

Figure 2.3. A schematic of the capillary array doser.

2.4 Reflection-Absorption Infrared Spectroscopy

Reflection-absorption infrared spectroscopy (RAIRS) is a very sensitive technique for the detection of organic functional groups, such as C=C, C=O and C-H.[47] These organic functional groups are characterized in infrared spectroscopy by the vibrational frequencies of the specific bond, which is related to the reduced mass and the bond strength, as shown in Equation (2.1)[48]:

$$\nu = 1/2\pi\,(k/\mu)^{1/2} \tag{2.1}$$

The fundamental principles of RAIRS are similar to those of traditional Fourier transform infrared spectroscopy (FTIR). A key component of both RAIRS and FTIR is the interferometer, where a beamsplitter transmits some light and reflects some light, resulting in constructive or destructive interference at the detector. The interferogram, which is the sum of contributions from all source wavelengths, can be converted to a frequency-domain spectrum after performing Fourier transform.[49] However, unlike FTIR of bulk materials, RAIRS obeys a surface selection rule, which was first described by Greenler.[47] Figure 2.4 shows a scheme of infrared radiation reflecting off a surface at an incident angle φ. IR radiation reflected off a substrate surface can be resolved into two components: p-polarized light (E_p), which is parallel to the incident plane, and s-polarized light (E_s), which is perpendicular to the incident plane. When

the p-polarized light is reflected off the substrate surface, it undergoes an incident angle-dependent phase change. In contrast, light that is polarized perpendicular to the incident plane (s-polarized light) undergoes a phase change of 180° at all angles of incidence. This phase shift causes destructive interference, which results in canceling out of s-polarized light after reflection.[47] The intensity of IR transitions is directly proportional to the square of the dot product of the transition dipole moment, $\boldsymbol{\mu}$, and the electronic field, **E**. Because the dot product is proportional to the cosine value of the angle between the two vectors and the electric field vector, **E**, is oriented perpendicular to the surface following reflection, only molecular vibrations with the transition dipole moment perpendicular to the surface can be observed in RAIRS. Furthermore, the largest absolute value of **E** is obtained from a 90° of phase change of the p-polarized light which occurs at an angle of 86°.[47]

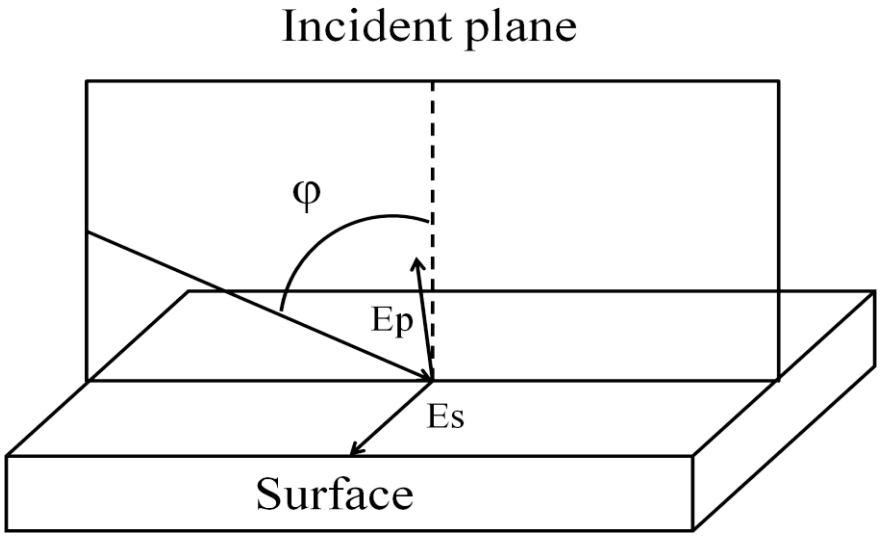

Figure 2.4. Infrared light reflecting from a substrate surface at the incident angle φ.

In this work, *in situ* RAIRS measurements were performed using a Bruker IFS 66v/S spectrometer attached to the UHV chamber. Focused IR radiation from a SiC

globar source was reflected off the gold surface at ~86 ° relative to the surface normal through a KBr window attached to the chamber. Then the IR radiation exited the chamber through another KBr window and was focused into a mid-range (750-4000 cm^{-1}) mercury cadmium telluride (MCT) detector, which was cooled by liquid nitrogen. All spectra shown in this thesis were obtained using 100 scans and a 2 cm^{-1} resolution with a scanner velocity of 20.0 kHz. All spectra were presented with the intensity defined as $-\log(R/R_0)$, where R was the reflectivity of the monolayer and R_0 was the reflectivity of a reference.

2.5 X-ray Photoelectron Spectroscopy

X-ray Photoelectron Spectroscopy (XPS) is a sensitive technique for surface analysis. It can determine the identity of surface-bound molecules and provide information about the local chemical environment of elements on substrates. XPS is based on Einstein's photoelectric effect, which states that electrons can be ejected from a metal surface by photons with sufficient energy.[50] The elemental identity and local chemical environment can be determined by the binding energy of the ejected photoelectron (E_b). This binding energy is related to the energy of incident photon ($h\nu$), the kinetic energy of the photoelectron (E_k) and the work function of the instrument (Φ), as shown in Equation (2.2) and illustrated in Figure 2.5:[51]

$$E_k = h\nu - \Phi - E_b \tag{2.2}$$

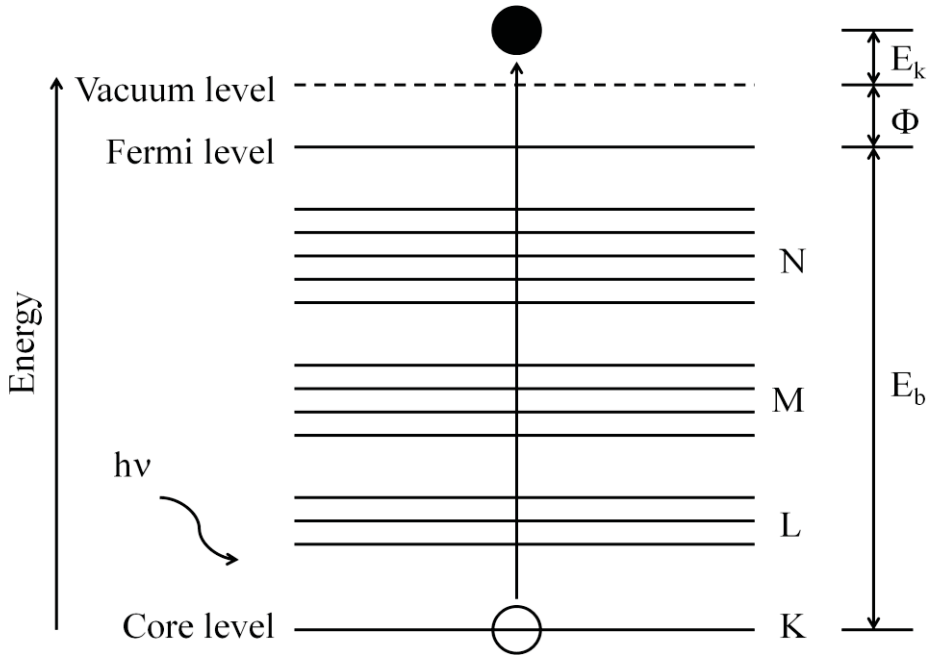

Figure 2.5. Energy level diagram of an ejected photoelectron. E_k is the kinetic energy of the photoelectron, E_b is the binding energy of the electron and Φ is the work function of the instrument.

In this thesis, radiation made by relaxation of Mg K electrons from higher level to lower level state (1253.6 eV) was generated from a SPECS X-ray source operating at 250 W (12.5 kV and 20 mA). Ejected photoelectrons were detected using a hemispherical energy analyzer (Perkin-Elmer) operating with pass energies between 20-50 eV. Survey spectra were collected with a resolution of 1 eV, and high resolution spectra with a step size of 0.1 eV were collected. All spectra were collected with a take-off angle of 45˚ with respect to the surface normal. The binding energies for all spectra were referenced to the Au($4f_{7/2}$) peak at 83.8 eV.

2.6 Summary

To study reactions that occur at the gas-surface interface, a well-defined condition and the incorporation of surface-sensitive techniques are essential. The ultrahigh

vacuum experiments were designed for this purpose. The surface reactions were monitored *in situ* with RAIRS. Using XPS, the surface was characterized before and after NO_3 exposure. Desorbed products could be detected in mass spectrometer.

Chapter 3

Reactions of Nitrate Radicals with Alkanethiol and Vinyl-terminated Self-Assembled Monolayers

3.1 Introduction

The nitrate radical is an important oxidizing gas in the atmosphere, which can initiate reactions with organics at night. Organic aerosols are ubiquitous in the environment and have many sources, such as biogenic emission from vegetation, fossil fuel combustion from automobiles, and secondary organic aerosols formed through reactions between volatile organic compounds and atmospheric oxidants, including nitrate radicals. Many studies have been focused on gas-phase reactions between nitrate radicals (NO_3) and organic compounds.[18,21,23,24,30-32] However, few investigations have contributed to exploring reactions of NO_3 with organic surfaces. The research in this thesis is aiming to develop an initial understanding of the reaction kinetics and mechanism between NO_3 and organic surfaces, such as alkanethiol and vinyl-terminated self-assembled monolayers.

Self-assembled monolayers (SAMs) have diverse applications in the fields of sensors, corrosion protection, nanofabrication, construction of nanodevices, medical implants and pharmacology.[52,53] Because SAMs are easily prepared and provide control over the surface order, orientation, and terminal functional group, they are often widely used as model organic surfaces. The most extensively studied monolayers are alkanethiol SAMs on gold substrates, for its inert nature that allows substrates to be manipulated in the air without oxidation. The sulfur head group and

the gold substrate are bonded in the form of a metal thiolate.[54] The well-ordered monolayer forms a (√3 X √3) R30° overlayer structure with the spacing between adjacent sulfur atoms equal to 4.99 Å.[55] This distance is greater than the distance of the closest approach of the methylene chains, so the chains tilt ~30° away from the surface normal to maximize the Van der Waals interactions.[56] The strong S-Au bond, 44 kcal mol^{-1}, generates a stable surface while the Van der Waals interactions between alkyl chains, 1-2 kcal mol^{-1}, ensures a tightly packed monolayer.[57]

My research objectives are to develop an initial understanding of the kinetics and the route for reactions of NO_3 with the well-defined organic surfaces. Based on the kinetic data, the initial reaction probability can be determined for NO_3 collisions with a vinyl-terminated SAM. These goals were accomplished by monitoring the changes of the monolayers on polycrystalline gold substrates during exposure to NO_3. The monolayers were characterized by Reflection-Absorption Infrared Spectroscopy (RAIRS) and X-ray Photoelectron Spectroscopy (XPS). Elemental analysis and oxidation state determination were performed with XPS.

3.2 Experimental Details

3.2.1 Materials

All chemicals were used as received without further purification unless otherwise noted. HPLC grade hexane was obtained from Fisher Scientific Inc. HPLC grade ethanol was purchased from Decon Laboratories, Inc. 1-decanethiol (96%), 1-pentadecanethiol (98%), 1-octadecanethiol (98.5+%), nitrogen monoxide (98.5%),

and nitrogen dioxide (99.5%) were purchased from Sigma-Aldrich, Inc. 14-pentadecene-1-thiol and 17-octadecene-1-thiol were synthesized by Jessica Weidgin Lu following the procedures of Hu and Fox.[58] Research grade oxygen, ultrahigh purity nitrogen, and dry ice were obtained from Airgas Specialty Gases. Polycrystalline gold substrates were purchased from Evaporated Metal Films.

3.2.2 Nitrate Radical Synthesis and Storage

A detailed description of how NO_3 were synthesized and stored was previously described in Chapter 2 and a brief description is presented here. Research grade oxygen was passed through a commercial ozone generator (RMU16-DG3 Ozone Generator Frame System). A mixture of O_2/O_3 (0.08 ppm of O_3) from the output of a commercial ozone generator was admitted through a previously dried glass vessel where it was mixed with nitrogen monoxide to produce N_2O_5. Once N_2O_5 was formed from the mixture with excess O_3, the resultant N_2O_5 was introduced into a glass trap submerged in a dry ice/ethanol bath. This procedure took approximately 2 hours. The N_2O_5 trap was then isolated and the dry ice was removed. As described in Chapter 1, NO_3 can be made by thermal decomposition of N_2O_5 (reaction (1.4)), and the equilibrium constant is related to the heating temperature (Equation (1.5)). The isolated trap was attached to the UHV chamber described in Chapter 2. The flowing N_2O_5 gas was heated to ~324 K before being introduced into the chamber. The concentration of NO_3 in the TDC was determined from Equation (1.5) and Equation (1.7) in Chapter 1.

3.2.3 Synthesis of Self-Assembled Monolayers and Monolayer Exposure

Polycrystalline gold substrates were immersed in a piranha solution (7:3 ratio, sulfuric acid/30% hydrogen peroxide) for ~45 min to remove most surface contaminates. The Au surfaces were then taken out of the piranha solution and rinsed thoroughly with deionized water (Millipore Purification Systems, 18.2 MΩ). Each substrate was then dried with a stream of ultrahigh pure nitrogen and immediately placed in a ~1 mM of the appropriate thiol solution in hexanes for about 24 hours. Before the exposure of SAMs to NO_3, the surface was first removed from the thiol solution and rinsed with hexanes. The monolayer was then dried in a stream of ultrahigh purity nitrogen and transferred into the ultrahigh vacuum chamber. The sample was aligned for RAIRS measurement with a precision manipulator. NO_3 were introduced into the UHV chamber through a capillary which was attached to a custom-made all-glass effusive molecular beam doser.

3.2.4 Reflection-Absorption Infrared Spectroscopic Measurement

Reactions between NO_3 and SAMs were monitored *in situ* using a Bruker IFS 66v/S spectrometer attached to the UHV chamber. Focused IR radiation from a SiC globar source was reflected off the gold surface at ~86 ° relative to the surface normal through a KBr window attached to the chamber. Then, the reflected radiation was detected by a mid-range (750-4000 cm^{-1}) mercury cadmium telluride (MCT) detector, which was cooled by liquid nitrogen. All spectra shown in this thesis were obtained using 100 scans and a 2 cm^{-1} resolution with a scanner velocity of 20.0 kHz. All

spectra were presented with the intensity defined as $-\log(R/R_0)$, where R was the reflectivity of the monolayer and R_0 was the reflectivity of a reference. To characterize the SAMs, a reference spectrum of a clean gold slide was used. After being immersed in a piranha solution for ~45 min, the cleaned Au surface was rinsed thoroughly with deionized water, and then was dried with a stream of ultrahigh purity nitrogen. To characterize the surface exposed to NO_3, the reference spectrum used was that of the SAM before NO_3 exposure. Spectra recorded with this type of reference were referred to difference spectra. The reaction kinetics was studied by recording IR spectra every 90 seconds during the NO_3 exposure.

3.2.5 X-ray Photoelectron Spectroscopic Measurements

The SAMs were characterized before and after NO_3 exposure with X-ray Photoelectron Spectroscopy (XPS). Radiation made by relaxation of Mg K electrons from higher level to lower level state (1253.6 eV) was generated from the X-ray source operating at 250 W (12.5 kV and 20 mA). Ejected photoelectrons were detected using the hemispherical energy analyzer which was operating with a pass energy of 50 eV. Survey spectra were collected with a resolution of 1 eV. Spectra of S(2p), N(1s), O(1s), C(1s), Au(4f) with a higher resolution of 0.1 eV were collected. The binding energy for all spectra was referenced to the $Au(4f_{7/2})$ peak at 83.8 eV.

3.3 Results and Discussion

3.3.1 Reaction Kinetics and Mechanism of NO_3 with an 18-carbon (18C) Vinyl-terminated SAM

The kinetics and mechanism for reactions between NO_3 radicals and an 18C vinyl-terminated SAM were investigated using the UHV system. The well-organized, thin, organic film was characterized with RAIRS before NO_3 exposure. During the exposure, oxidation of the surface by NO_3 was monitored *in situ*. The oxidation states of surface-bound products were analyzed by XPS. The reaction kinetics and mechanism will be discussed in details below.

3.3.1.1 Monolayer Characterization

3.3.1.1.1 Reflection-Absorption Infrared Spectroscopic Data

Figure 3.1 shows the reflection-absorption infrared spectrum of an 18C vinyl-terminated SAM on a polycrystalline gold substrate before NO_3 exposure. The intensity is defined as $-\log(R/R_0)$ where R is the reflectance of the SAM and R_0 is the reflectance of a clean gold substrate. Mode assignments are shown in Table 3.1.[59-61]

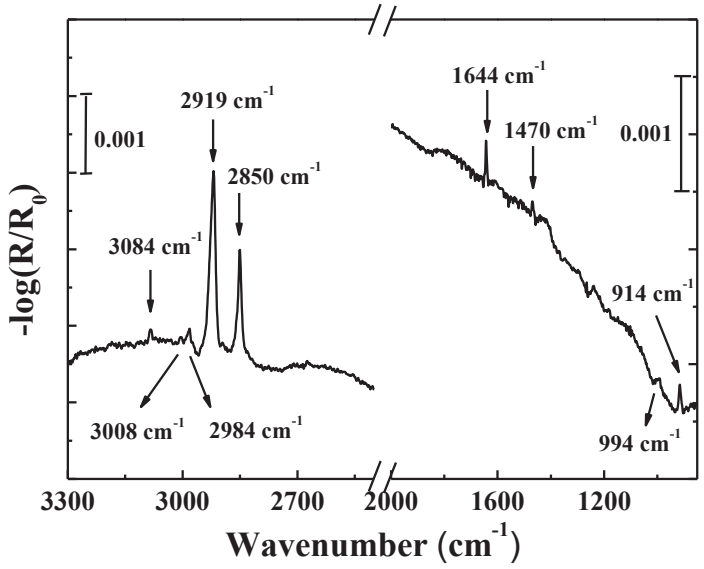

Figure 3.1. A reflection-absorption infrared spectrum with band assignments of an 18C vinyl terminated SAM.

The most intense peaks in Figure 3.1 are due to the asymmetric and symmetric CH_2 stretches at 2918 and 2849 cm^{-1}, respectively. In a polyethylene crystal, the asymmetric and symmetric CH_2 stretches are found at 2920 and 2850 cm^{-1}.[62] Because the positions of these two peaks are considered to be a sensitive indicator of the order of the alkyl chains,[54,57] the peak positions for the asymmetric and symmetric CH_2 stretches and the sharp peak shapes in Figure 3.1 indicate a well-ordered 18C vinyl-terminated SAM formed on Au.

Six of the bands associated with the terminal vinyl group are observed in Figure 3.1.[59] The peaks at 3084 and 2984 cm^{-1} are assigned to the asymmetric and symmetric CH_2 stretches of the $=CH_2$ group, respectively. The peak at 3008 cm^{-1} is assigned to the β C-H stretch of the $–HC=CH_2$ group. The mode found at 1644 cm^{-1} is attributed to the C=C stretch. The small peak at 994 cm^{-1} is assigned to the out-of-plane deformation (oop def) of the C=C group. The larger band at 914 cm^{-1} is assigned to

the out-of-plane deformation of the $=CH_2$ group.

Table 3.1. RAIR spectroscopic band positions and vibrational mode assignments for an 18C vinyl-terminated SAM on Au.

Wavenumber (cm^{-1})	Vibrational Modes
3084	$\nu_a(=CH_2)$
3008	$\nu(H\text{-}C=CH_2)$
2984	$\nu_s(=CH_2)$
2918	$\nu_a(CH_2)$
2849	$\nu_s(CH_2)$
1644	$\nu(C=C)$
994	C=C oop def
914	$\omega(=CH_2)$

3.3.1.1.2 Reactivity of Vinyl-terminated SAMs toward NO/NO_2

In Chapter 2, it has been discussed that NO_3 were generated from the thermal decomposition of N_2O_5 accompanied with the formation of NO_2. In addition, NO_3 can be photolysed by visible light to produce some amount of NO. To determine whether NO/NO_2 would interfere with our measurement of the initial reaction probability, a 15-carbon (15C) vinyl-terminated SAM was exposed to the pure NO/NO_2 for 30 min. The results from these studies are provided in Figure 3.2 and Figure 3.3.

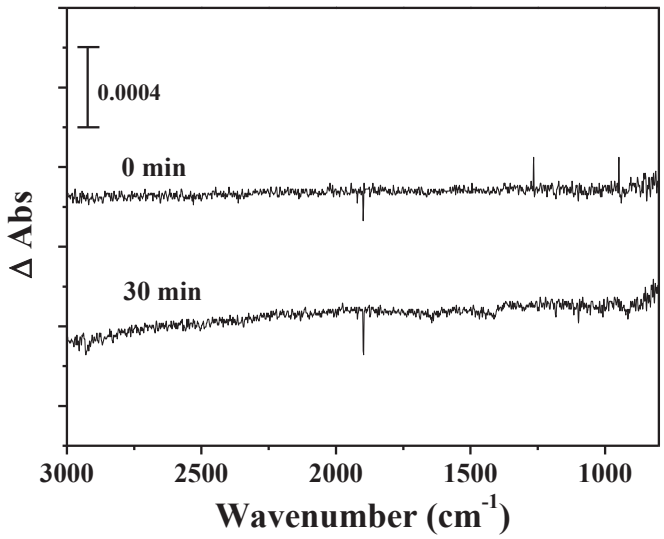

Figure 3.2. Reflection-absorption infrared difference spectra of a 15C vinyl-terminated SAM before and after NO exposure. The top spectrum is the monolayer with no NO exposure, and the bottom spectrum is the one with 30 min of NO exposure.

Figure 3.2 shows RAIR difference spectra of a 15C vinyl-terminated SAM before and after exposure to the pure NO for 30 min. The reference spectrum (R_0) is that of the monolayer before any exposure. The top spectrum is that of the monolayer before exposure to NO, and the bottom one is that of the monolayer after 30 min of exposure to NO. No negative features in the C-H stretch region and at the position associated with the C=C group are observed in this figure. There are also no positive peaks observed within the limit of detection. Therefore, the reactivity of the vinyl-terminated SAM toward NO appears to be very low.

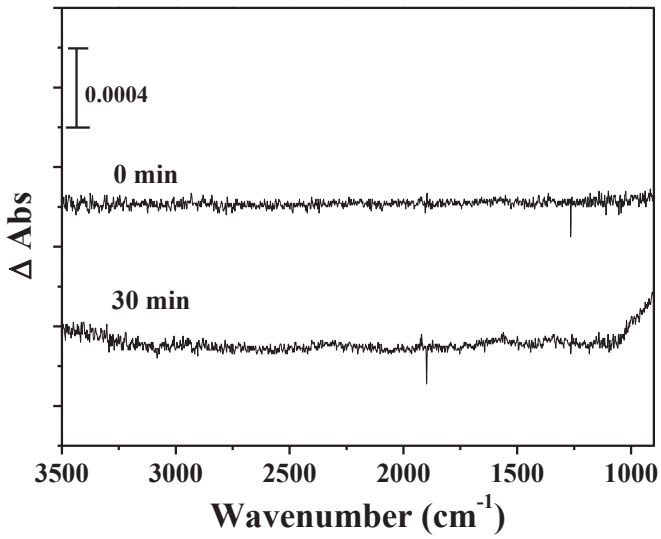

Figure 3.3. Reflection-absorption infrared difference spectra of an 18C vinyl-terminated SAM before and after NO_2 exposure. The top spectrum is the monolayer with no exposure of NO_2, and the bottom spectrum is the one with 30 min of NO_2 exposure.

Figure 3.3 shows the RAIR difference spectra of a 15C vinyl-terminated SAM before and after exposure to the pure NO_2. The reference spectrum (R_0) is the same as the one in Figure 3.2. The top spectrum is that of the monolayer before exposure to NO_2, and the bottom one is that of the monolayer after 30 min of exposure to NO_2. The spectrum is almost unchanged either at bands related to the double bond or in the C-H stretch region after exposure within the limit of detection. Therefore, we can conclude that the changes in IR spectra during NO_3 exposure are not due to reactions between the monolayer and NO/NO_2, but rather the reaction of the surface with NO_3.

3.3.1.3 RAIRS during NO_3 Exposure

Oxidation of the vinyl-terminated SAM by NO_3 was monitored using *in situ* RAIRS. Figure 3.4 shows a subset of time-resolved RAIR spectra of an 18C

vinyl-terminated SAM during NO_3 exposure. The reference spectrum is that of the monolayer before exposure. The bottom spectrum in Figure 3.4 is the difference spectrum of the monolayer before exposure. From the bottom toward the top of this figure, exposure of the monolayer to NO_3 increases by 3×10^2 L per scan with the top spectrum obtaining a total exposure of 5×10^3 L of NO_3. The first observable changes in the RAIR spectrum of the 18C C=C SAM upon exposure to NO_3 (see the second spectrum from the bottom in Figure 3.4) are a decrease in signal at 3084 cm^{-1}, 1644 cm^{-1}, and 914 cm^{-1}. The decrease in intensity of these modes is caused by a reaction that occurs between the monolayer and the terminal C=C moiety. At the same time the bands associated to the C=C group decrease, positive peaks emerge at 1620 cm^{-1}, 1280 cm^{-1}, 850 cm^{-1}, and 1555 cm^{-1}, which are assigned to the asymmetric and symmetric NO_2 stretches of organic nitrates, the NO stretch of organic nitrates, and the asymmetric NO_2 stretch of nitro compounds,[61,63] indicating that the reaction of NO_3 with the vinyl-terminated monolayer forms a species which contains organic nitrates or nitro compounds. The small peaks at 1230 cm^{-1} and 1450 cm^{-1} are likely due to the C-O stretch and the CH_2 deformation of epoxides produced during the reaction.[61]

The only other change observed in the spectra of Figure 3.4 is the formation of two negative peaks in the hydrocarbon region, indicating H possible abstraction from the monolayer during NO_3 exposure, or the chain reorientation due to reactions of the double bond with NO_3, or the chain desorption from the surface due to the oxidation of sulfur on the gold substrate. Upon continuous exposure to NO_3, positive peaks

appear adjacent to the hydrocarbon region. Since the position of the peaks from the asymmetric and symmetric CH_2 stretches has been shown to be a sensitive indicator of the order of the methylene chains,[54,57] the shift of the two peaks to higher wavenumbers indicates a disordering within the alkyl chains upon exposure to NO_3, which aligns the methylene stretches in directions that can be detected by RAIRS.

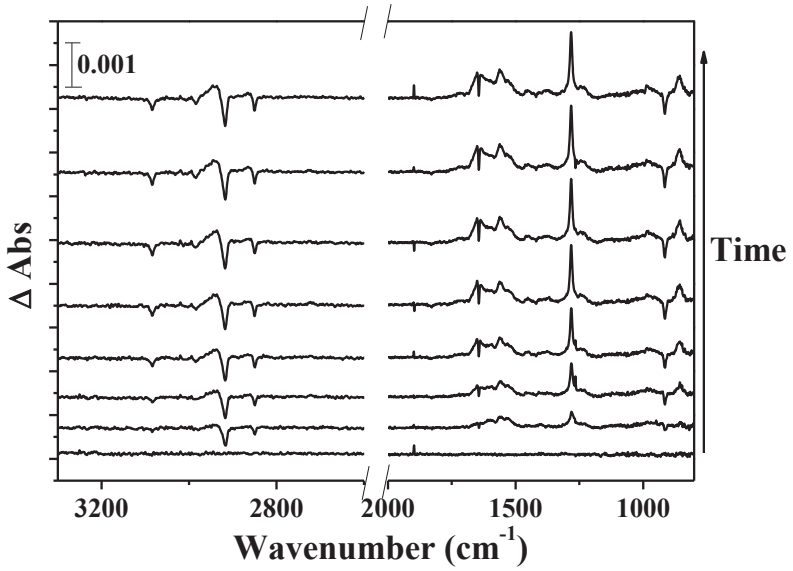

Figure 3.4. Reflection-absorption infrared difference spectra of an 18C vinyl-terminated SAM during NO_3 exposure The bottom spectrum is the monolayer with no NO_3 exposure, and the exposure increases by 3×10^2 L per spectrum from bottom to top with a total dose of 5×10^3 L of NO_3.

3.3.1.4 Reaction Kinetics between NO_3 and the 18C Vinyl-terminated SAM

The previous section provides important information about the likely functional groups formed on the surface and the possible pathways during reactions, a complete mechanistic understanding of the reaction requires more detailed analysis of the reaction kinetics. To learn about the oxidation kinetics for the reaction between gas-phase NO_3 and the 18C vinyl-terminated SAM by NO_3, the data was analyzed by plotting the intensity of the band from the C=C stretch at 1644 cm^{-1} versus the

exposure time in Figure 3.5. During NO_3 exposure, the position of this band remains constant, so the change in intensity of the band is proportional to the change in concentration of the double bonds (within the limit of Beer's law). The figure shows that the band intensity from the C=C stretch decreases exponentially during NO_3 exposure. Based on the pseudo-first-order kinetics, the rate of consumption of the C=C groups should lead to a simple exponential decay in the intensity of the signal at 1644 cm^{-1}according to:

$$A(t) = A_0 \exp(-k_{obs}t), \tag{3.1}$$

where $A(t)$ is the absorbance of the band from ν(C=C) at any time and A_0 is the initial absorbance of the same band. k_{obs} is the observed rate constant for the consumption of carbon-carbon double bonds and t is the time of exposure to NO_3 in seconds. From the best non-linear least squares fit to the data, the rate constant is determined to be (1.4 ± 0.3) X 10^{-3} s^{-1}.

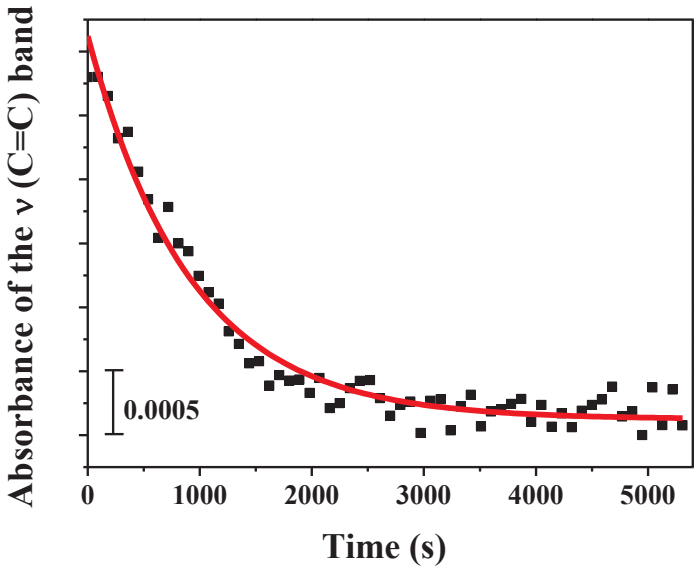

Figure 3.5. A graph of the absorbance of the band from ν(C=C) at 1644 cm^{-1} versus the time of NO_3 exposure. The solid red line is the fit to the data to determine the observed rate constant (see text for details).

In addition to the rate of the double bond consumption, we have used the IR data from Figure 3.4 to learn about the rate for product formation. Figure 3.6 shows a graph obtained by plotting the intensity of the band from the symmetric NO_2 stretch of organic nitrates at 1280 cm^{-1} versus the exposure time. Similar to the exponential decay in the signal at 1644 cm^{-1}, the intensity of the band at 1280 cm^{-1} increases exponentially with exposure to NO_3. Because the change in intensity of the band is most likely proportional to the change in concentration of organic nitrates formed during the reaction (within the limit of Beer's law), according to the pseudo-first-order kinetics of organic nitrates formation, the change in the signal can be modeled with Equation (3.2):

$$A(t) = A_0 [1 - \exp(-k_{obs}t)], \tag{3.2}$$

where $A(t)$ is the absorbance of the band from $\nu_s(\text{-}ONO_2)$ at any time and A_0 is the initial absorbance of the same band. k_{obs} is the observed rate constant for the formation of organic nitrates and t is the time of exposure to NO_3 in seconds. The best fit to the data yields an observed rate constant of $(1.3 \pm 0.2) \times 10^{-3}$ s^{-1}, which is identical, within the error, to the observed rate constant for the consumption of the C=C group. Therefore, the consumption of the double bonds must lead directly to the production of organic nitrates upon NO_3 exposure.

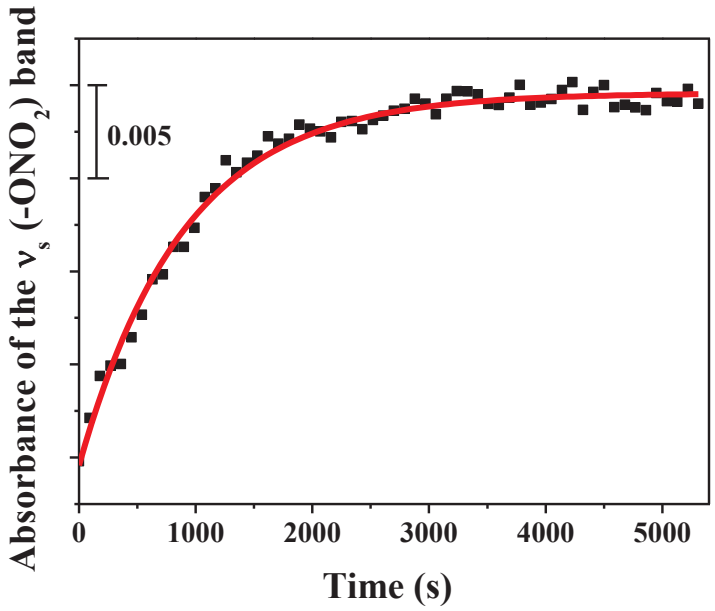

Figure 3.6. A graph of the absorbance of the band from ν_s(-ONO_2) at 1280 cm^{-1} versus the time of NO_3 exposure. The solid red line is the fit to the data to determine the observed rate constant (see text for details).

To determine the initial reaction probability, we modeled the change in intensity of ν_s(-ONO_2) at 1280 cm^{-1} according to simple Langmuirian kinetics (first-order reaction model):[42]

$$A(t) = A_0 [1 - \exp(-\alpha t)], \quad (3.3)$$

where $A(t)$ is the band absorbance from ν_s(-ONO_2) at any time, and A_0 is the initial absorbance of the same band before exposure to NO_3. The time of exposure to NO_3 in seconds is represented as t, and α can be determined from Equation (3.4):[42]

$$\alpha = (1/4 \langle v \rangle \gamma_0 [NO_3]_g) / L \quad (3.4)$$

Here, $\langle v \rangle$ is the mean molecular velocity of NO_3 in cm/s, γ_0 is the initial reaction probability, $[NO_3]_g$ is the gas-phase NO_3 concentration adjacent to the surface, and L is the initial surface coverage of the carbon-carbon double bonds. The gas-phase NO_3 concentration in the TDC was estimated from the equilibrium constant in Equation

(3.5)[18,19] and Equation (3.6):

$$K_{eq} = 2.7 \times 10^{-27} \times \exp(11000K/T)\ cm^3\ molecule^{-1} \quad (3.5)$$

$$[N_2O_5] = K_{eq} \times [NO_2] \times [NO_3] \quad (3.6)$$

where T is the heating temperature equal to 324 K. At any time during decomposition of N_2O_5, the concentration of NO_3, $[NO_3]$, was equal to the concentration of NO_2, $[NO_2]$, within the TDC of the doser. Therefore, at equilibrium, the number density of NO_3 in the TDC could be determined from the equilibrium constant, K_{eq}, and the concentration of N_2O_5. Because the flux at the input of the doser was equal to the flux in the TDC, the flux of N_2O_5, 2×10^{15} molecule s^{-1}, was determined from Equation (3.7):[64]

$$F = n\,C = 1/4\ n \langle v \rangle A \quad (3.7)$$

where F is the flux of N_2O_5, n is the number density of gas molecules, C is the conductance (calculated from the known size of the aperture in the capillary) through the capillary of the doser, 4×10^{-4} L s^{-1}, $\langle v \rangle$ is the velocity of gas molecules, and A is the area of the aperture entering the TDC, 0.24 cm^2. By taking the equilibrium between N_2O_5 and NO_3 into account, the effective flux of NO_3 at the surface was calculated to be 1×10^{15} molecules s^{-1}. Therefore, the concentration of NO_3 radicals adjacent to the surface, $[NO_3]_g$, was determined to be 3×10^{10} molecules cm^{-3} from Equation (3.7). The initial surface coverage of C=C bonds was assumed to be the same as the coverage of methyl-terminated monolayers, 4.7×10^{14} molecules cm^{-2}.[54] This assumption was reasonable because vinyl-terminated SAMs appeared to be similar in number density, size, and shape to alkanethiol SAMs.[59] From the model fits,

the initial reaction probability for NO_3 with an 18C vinyl-terminated SAM was calculated to be $(3 \pm 1) \times 10^{-3}$. Our observation reveals that there are three reactions that occur in every ~1000 gas-phase collisions between NO_3 and the carbon-carbon double bond.

The experiment-determined reaction probability of NO_3 with the vinyl terminated monolayer is over an order of magnitude smaller than that obtained recently by Bertram et al.. In the experiments, they employed a SAM-coated flow reactor, which was used to report a reaction probability of 3.4×10^{-2}.[43] This difference could result from three reasons. Firstly, Bertram Group used the loss of NO_3 during the reaction to estimate the reaction probability. When exposing the SAM to NO_3, it could undergo a variety of reactions such as hydrogen abstraction except for electrophilic addition. Secondly, they studied reactions of NO_3 with an 11C vinyl terminated SAM on a cylindrical gold coated tube. Inherently, the vinyl-terminated monolayer with a shorter chain length creates more defects on the surface, which could also increase the reaction probability of the organic surface with NO_3. Thirdly, the measurement of the reactive uptake coefficient was performed in the presence of O_2 and was not controlled under the vacuum. In the proposed mechanism, O_2 can oxidize the alkyl radical to produce a nitroxy peroxyl radical, which is considered to undergo further reaction with NO_3.[43] This may be another factor that increases the reaction probability in their work. In addition, the initial reaction probability obtained in this thesis is approximately two orders of magnitude higher than that for the reaction of ozone with the same SAM, indicating that the reactivity of NO_3 is much higher than that of

ozone.[65] This may be because the electrophilic addition of NO_3 can take place at positions where the radical on the oxygen atom can interact with the double bond, while ozone has to collide with the double bond in the direction favorable to form the primary ozonide, which increases the reaction barrier compared to that of the reaction between the same surface and NO_3.

3.3.1.5 Characterization of the surface after NO_3 Exposure

Figure 3.7 shows RAIR spectra of an 18C vinyl-terminated SAM before and after exposure. The spectrum of Figure 3.7 B is that of the monolayer after exposure to 5 X 10^3 L of NO_3. The spectra are offset along the vertical axis for clarity. It should be noticed that the disappearance in signal from the asymmetric and symmetric CH_2 stretches of $=CH_2$ at 3084 and 2984 cm^{-1}, the β C-H stretch of $-HC=CH_2$ at 3008 cm^{-1}, the stretch of C=C at 1644 cm^{-1}, and the out-of-plane deformation of $=CH_2$ at 914 cm^{-1}, all indicate extensive reaction of the double bond with the impinging NO_3. A broadening and decrease in the intensity of the modes from the asymmetric and symmetric CH_2 stretches of methylenes are also noticeable after NO_3 exposure, which could result from chain reorientation due to reactions at the double bond, or hydrogen abstraction by NO_3 from $-CH_2$, or chain desorption from the surface due to oxidation of sulfur by NO_3. The new broad feature at 1615-1650 cm^{-1} and the new sharp peak at 1283 cm^{-1} are assigned to the asymmetric and symmetric NO_2 stretches of the $-ONO_2$ group.[31,63] In the previous section, the kinetic data showed that the consumption of the double bonds led directly to the formation of organic nitrates upon NO_3 exposure.

Therefore, the peaks at the hydrocarbon region broaden and decrease probably because of chain reorientation due to reactions at the double bond upon NO_3 exposure. In addition, we attribute the peak at 1555 cm^{-1} to the asymmetric NO_2 stretch of nitro compounds.[31,63]

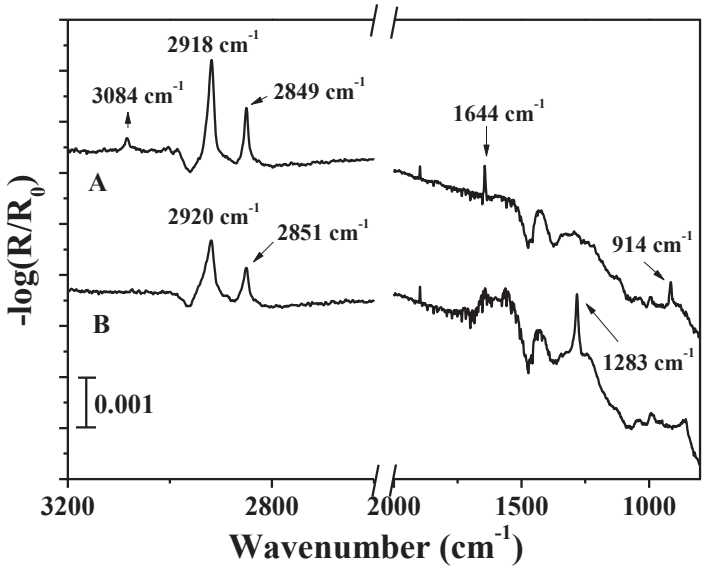

Figure 3.7. Reflection-absorption infrared spectra of an 18C vinyl-terminated SAM before and after exposing the surface to NO_3 radicals. The top spectrum (A) is the monolayer before exposure to NO_3 and the bottom spectrum (B) is the monolayer after 1.5 hours of NO_3 exposure.

Further characterization of the 18C vinyl terminated monolayer was performed using X-ray Photoelectron Spectroscopy (XPS) to obtain information about the binding environments of the elements. Representative high resolution spectra of the S(2p), N(1s), O(1s) and C(1s) regions of an 18C vinyl-terminated SAM are shown in Figure 3.8. A high resolution X-ray photoelectron spectrum was recorded for the Au 4f region which was used as the reference for the binding energy of all other spectra shown in this work. The Au 4f spectrum consisted of a well-resolved doublet at 83.8 and 87.4 eV.

The S 2p region of the 18C vinyl-terminated SAM exhibits a peak centered at 163 eV before exposure, which is consistent with sulfur atoms bound to a gold substrate as the thiolate.[66] The intensity of the S 2p peak in the XPS spectrum shows little to no change following exposure of the surface to NO_3. This important observation indicates that the Au-S bond is not oxidized during NO_3 exposure and that reactions are likely isolated at the chain terminus. The binding energy at 400 eV in N 1s region indicates the formation of organic nitrates after 5×10^3 L of exposure.[67]

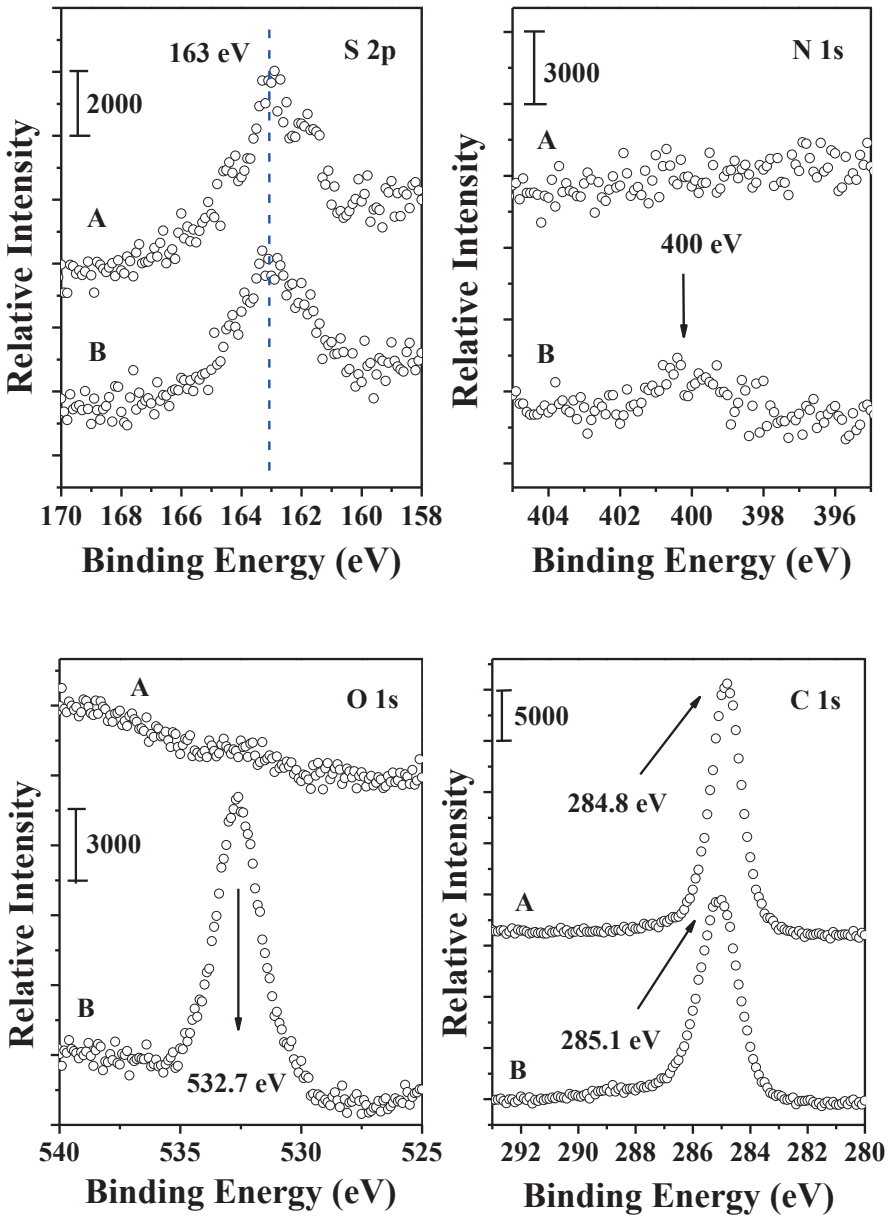

Figure 3.8. High resolution X-ray photoelectron spectra of the S(2p), N(1s), O(1s), and C(1s) regions of an 18C vinyl-terminated SAM A) before and B) after NO_3 exposure.

A high resolution X-ray photoelectron spectrum of the O 1s region of an 18C vinyl-terminated SAM is also shown in Figure 3.8. The vinyl-terminated monolayer shows no signal above noise for O 1s photoelectrons before exposure. After 1.5 hours of exposure to NO_3, a peak positioned at 532.7 eV indicates oxidized species formed on the surface. In addition, the relative intensity of N:O ratio is about 1:3, which

suggests the presence of $-ONO_2$ groups on the surface. The peak centered at 284.8 eV in the high resolution XPS spectrum of the C 1s region is in excellent agreement with the literature value of the binding energy for methylenes and terminal vinyl carbon atoms.[66] After NO_3 exposure, the peak broadens slightly when it shifts to a higher binding energy, which is indicative of the emergence of a new C-O species on the surface.[67]

3.3.1.6 Proposed Mechanism for Reactions of NO_3 with Vinyl-terminated SAMs

Similar to the gas-phase experiments,[2,27] the reaction of NO_3 with vinyl-terminated SAMs appears to be initiated by an electrophilic addition of NO_3 to the carbon-carbon double bonds, forming an alkyl radical adduct intermediate. Previous studies have proposed that the radical intermediate is unstable and will either decompose to an oxirane or collisionally stabilize. When the heterogeneous oxidation of the vinyl terminated SAM with NO_3 was monitored *in situ*, several significant changes were observed in RAIRS. The first change was the negative peaks emerging at bands from motions related to the double bond, which showed that the reaction consumed C=C moieties. Simultaneously, during the exposure of the vinyl-terminated monolayer to NO_3, peaks at 1280 cm^{-1}, ~1620 cm^{-1}, and 850 cm^{-1} from the symmetric and asymmetric NO_2 stretches and the NO stretch of organic nitrates,[61,63] indicated that oxidation of the monolayer by NO_3 produced $-ONO_2$ functional compounds, which was consistent with the XPS observation. The third significant change in RAIRS during the exposure of the vinyl-terminated monolayer to NO_3 was the

decrease of the bands from the $\nu_a(CH_2)$ and $\nu_s(CH_2)$ modes of the hydrocarbon chains. Upon further exposure of the monolayer to NO_3, positive peaks emerged adjacent to the bands of the hydrocarbon region. Because the position of the bands for the $\nu_a(CH_2)$ and $\nu_s(CH_2)$ modes has been shown to be a sensitive indicator of the order of the methylene chains,[54,57] the shifting of these bands to higher wavenumbers indicates that the orientation of the transition dipole moment of the motions from the methylene chains has changed during the reaction. The decrease in the intensity of the bands at hydrocarbon region might also be due to hydrogen abstraction from $-CH_2$ groups.

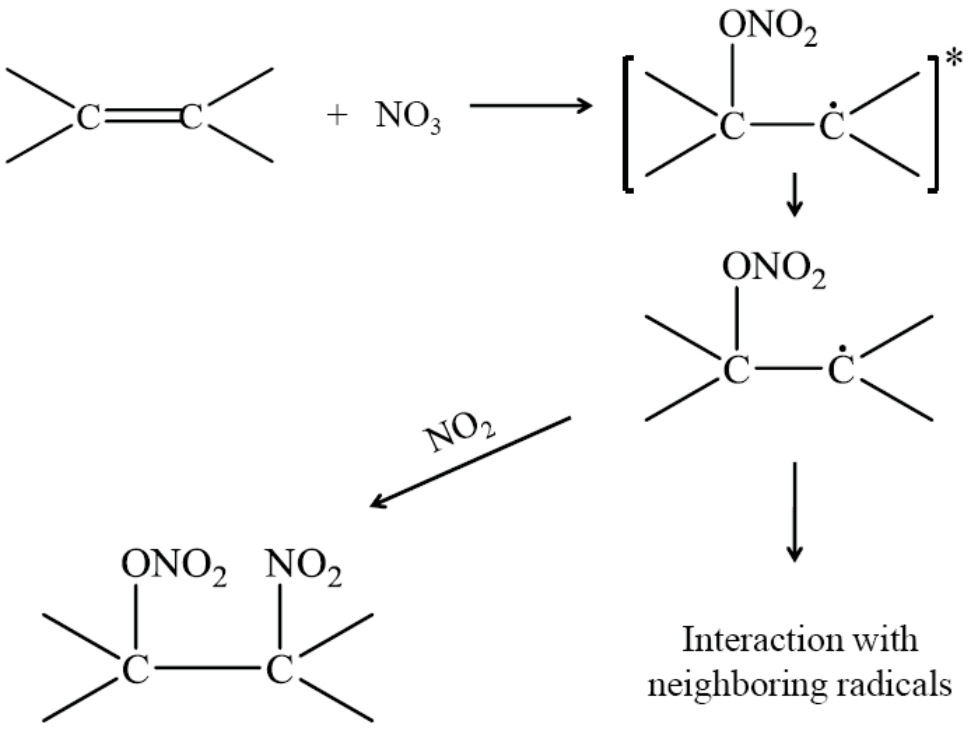

Figure 3.9. A scheme of the possible mechanistic pathways in which NO_3 can oxidize a terminal vinyl group bound to a surface.

In addition, bands at 1230 cm^{-1} and 1450 cm^{-1} possibly from the C-O stretch and the CH_2 deformation of epoxides might be due to the decomposition of the intermediate into an oxirane.[27,61] Another change in the IR data during exposure was

the positive peak that emerges at 1555 cm^{-1} from the asymmetric NO_2 stretch of nitro compounds.[61,63] It is proposed that the collisionally stabilized alkyl radical adduct intermediate can further react with NO_2 molecules, which are generated from thermal decomposition of N_2O_5, to form nitro compounds. The addition of NO_2 to the alkyl radical might result in the termination of possible radical propagation along the methylene chains. Moreover, the generated alkyl radical could also combine with neighboring radicals to form a new bond.

3.3.2 Reactions between NO_3 and Alkanethiol SAMs

In the previous section, we have discussed that the decrease in the intensity of bands at hydrocarbon region could result from chain reorientation due to reactions at the double bonds, or chain desorption due to oxidation of sulfur on Au by NO_3, or hydrogen abstraction from methylene groups. Although, XPS data proved that sulfur was not oxidized during NO_3 exposure, we were not able to determine if there was hydrogen abstraction during reactions. To explore this mechanism, we replaced the 18C vinyl-terminated SAM with an 18C methyl-terminated SAM and studied reactions of the methyl-terminated SAM with NO_3. The reaction mechanism will be discussed in more details below.

3.3.2.1 Monolayer Characterization

3.3.2.1.1 Reflection-Absorption Infrared Spectroscopic Data

Figure 3.10 shows the reflection-absorption infrared spectrum of an 18-carbon

(18C) methyl-terminated SAM on a polycrystalline gold substrate before exposure to NO_3. In this figure, the intensity is defined as $-\log(R/R_0)$ where R is the reflectance of the SAM and R_0 is the reflectance of a clean Au substrate.

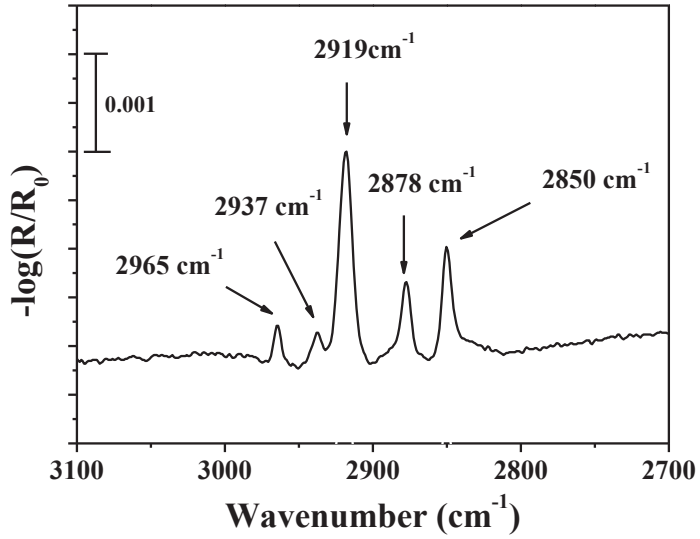

Figure 3.10. A Reflection-absorption infrared spectrum of an 18C methyl-terminated self-assembled monolayers.

It should be noticed first that the five important peaks in Figure 3.10 show a well-ordered monolayer formed on the gold substrate. They are assigned to the asymmetric stretch of CH_3, $\nu_a(CH_3)$, Fermi resonance of $\nu_s(CH_3)$ with low frequency CH_3 deformation mode, the asymmetric stretch of CH_2, $\nu_a(CH_2)$, the symmetric stretch of CH_3, $\nu_s(CH_3)$ and the symmetric stretch of CH_2, $\nu_s(CH_2)$ from high to low wavenumber, as shown in Table 3.2.[68] Since the position of the peaks from the CH_2 stretches is considered to be a sensitive indicator of the order of the alkyl chains,[57,59] the peaks at 2919 cm^{-1} and 2850 cm^{-1} indicate a well-ordered (crystalline-like) system. Secondly, it is interesting to note that the intensity of the CH_2 stretch is not 17 times bigger than that of CH_3 stretch as may be expected based on the fact that there are 17

CH_2 groups for every CH_3 group along a single chain. This is due to the fact that the transition dipole moment for the CH_2 stretch is not as perpendicular to the surface as that of CH_3. The so-called surface selection rule dictates that only those motions that produce a transition dipole moment perpendicular to the surface can be detected with RAIRS.

Table 3.2. Selected spectral positions and vibrational mode assignments for an 18C methyl-terminated SAM on Au.

Wavenumber (cm^{-1})	Vibrational Modes
2965	$\nu_a(CH_3)$
2937	$\nu_s(CH_3)$, Fermi resonance
2919	$\nu_a(CH_2)$
2878	$\nu_s(CH_3)$
2850	$\nu_s(CH_2)$

3.3.2.1.2 Reactivity of Alkanethiol SAMs toward NO/NO_2

In Chapter 2, it has been discussed that NO_3 were produced from the thermal decomposition of N_2O_5, accompanied with the formation of NO_2. In addition, photolysis of NO_3 by visible light generates some amount of NO. To determine if NO/NO_2 will interfere with our understanding of the reaction between NO_3 and the monolayer as well as to learn about the possible role of these molecules in the overall chemistry, a 15C methyl-terminated SAM was exposed to the pure NO/NO_2 for 30 min, as shown in Figure 3.11 and Figure 3.12.

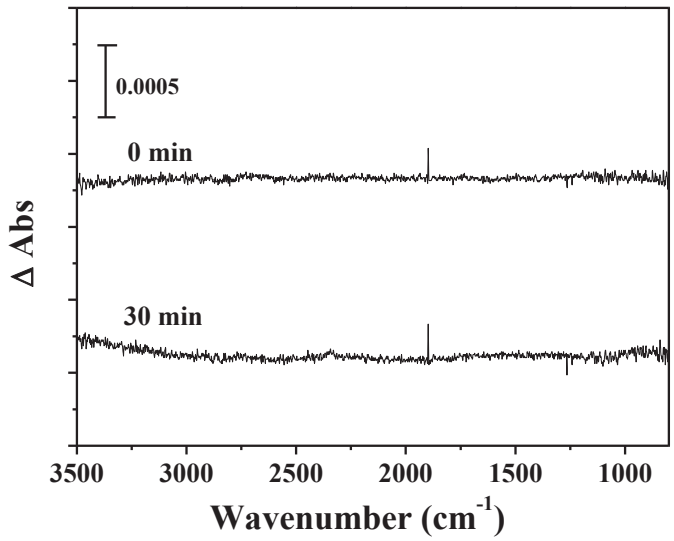

Figure 3.11. Reflection-absorption infrared difference spectra of a 15C methyl-terminated SAM before and after NO exposure. The top spectrum is that of the monolayer with no NO exposure, and the bottom spectrum is that of the monolayer with 30 min of NO exposure.

Figure 3.11 shows RAIR difference spectra of a 15C methyl-terminated SAM before and after exposure to the pure NO. The reference spectrum (R_0) for these spectra is that of the monolayer before any exposure. The top spectrum is that of the monolayer before exposure to NO, and the bottom one is that of the monolayer after 30 min of exposure to NO. There are clearly no changes above our signal-to-noise level in the two spectra. Therefore, the reactivity of the CH_3-terminated SAM toward NO appears to be very low.

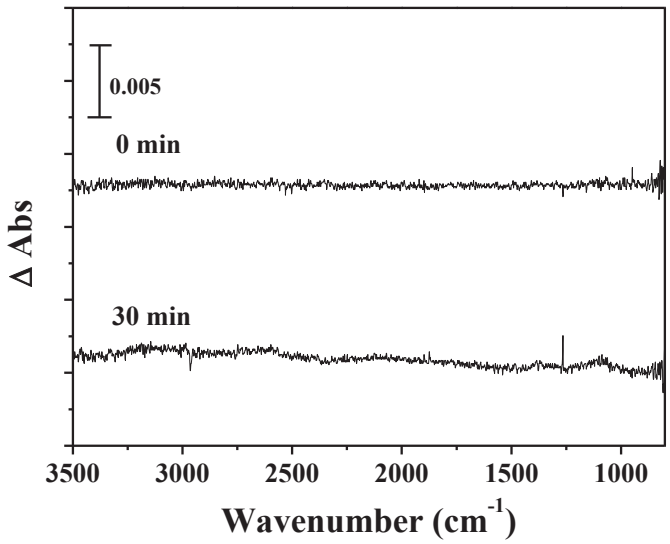

Figure 3.12. Reflection-absorption infrared difference spectra of a 15C methyl-terminated SAM before and after NO_2 exposure. The top spectrum is that of the monolayer with no NO_2 exposure, and the bottom spectrum is that of the monolayer with 30 min of NO_2 exposure.

Figure 3.12 shows the RAIR difference spectra of a 15C methyl terminated SAM before and after exposure to the pure NO_2. The reference spectrum (R_0) is the same as the one in Fig 3.11. The difference spectra are used in the experiments because even a very small change can be easily observed in the spectra. The top spectrum is that of the monolayer before exposure to NO_2, and the bottom one is that of the monolayer after 30 min of exposure to NO_2. After 30 min of exposure, the spectrum in the C-H stretch region is almost unchanged within the limit of detection. Therefore, we can conclude that a methyl-terminated SAM does not appear to react with NO or NO_2 on the time scale of our measurements.

3.3.2.2 RAIRS during NO_3 Exposure

Following our bench-mark studies with the background gases NO and NO_2, we

turn to studies with NO_3. To explore more details of the mechanism for reactions between SAMs and NO_3, we performed *in situ* RAIR spectroscopic experiments by exposing the 18C methyl-terminated SAMs to NO_3. Figure 3.13 shows a subset of the time-resolved RAIR spectra, with the spectrum of the monolayer before any exposure to NO_3 as the reference spectrum (R_0). These difference spectra are offset along the vertical axis for clarity and are arranged from bottom to top in increasing order of exposure to NO_3. The bottom spectrum is that of the monolayer before exposure. The exposure between each scan is 2×10^3 L.

The first changes in the spectra at early times are negative peaks attributed to the disappearance of asymmetric and symmetric methylene stretches. Both of the intensities decrease upon initial exposure to NO_3 suggesting hydrogen abstraction from methylenes by NO_3. With further NO_3 exposure, the positive features near the asymmetric and symmetric methylene stretches are clear evidence for the blue-shift of the peak frequencies of these modes. This shift is consistent with the transformation of an ordered system to a disordered system.

Concurrent with the formation of the negative peaks, a positive peak emerges at 2973 cm^{-1} which might be assigned to the C-H stretch of an alkyl radical $-CH-CH_3$ produced by hydrogen abstraction from a methylene group. This frequency red-shift about 30 wavenumbers compared to that for the C-H stretch (3008 cm^{-1}) from a vinyl group $-CH=CH_2$. The decrease in the frequency might be due to an increase of the reduced mass of the carbon attached to a $-CH_3$ group, compared to that attached to a $=CH_2$ group, or a decrease in the strength of the C-H bond because of an unpaired

electron on the carbon atom repelling the shared electrons of that C-H bond (Equation (2.1)). On the other hand, the positive peak could also be due to the symmetric stretch of a formed radical, $-CH_2$, from hydrogen abstraction of a methyl group. This proposed hydrogen abstraction from a methyl group is consistent with a decrease of the peak at 1380 cm^{-1} which is assigned to the symmetrical deformation vibration of $-CH_3$. To determine which pathway is more likely, isotopic experiments may be needed.

In addition, four positive peaks begin to develop at 1555 cm^{-1}, 1280 cm^{-1},1600 cm^{-1}, and 1230 cm^{-1}, which are assigned to the asymmetric NO_2 stretch of nitro compounds, the symmetric NO_2 stretches, the asymmetric NO_2 stretches of organic nitrates, and the C-O stretch respectively.[31,63] Upon further exposure to NO_3, these peak intensities change, which could result from the increase in the amount of product on the surface or the change in the orientation of motions from the formed functional groups.

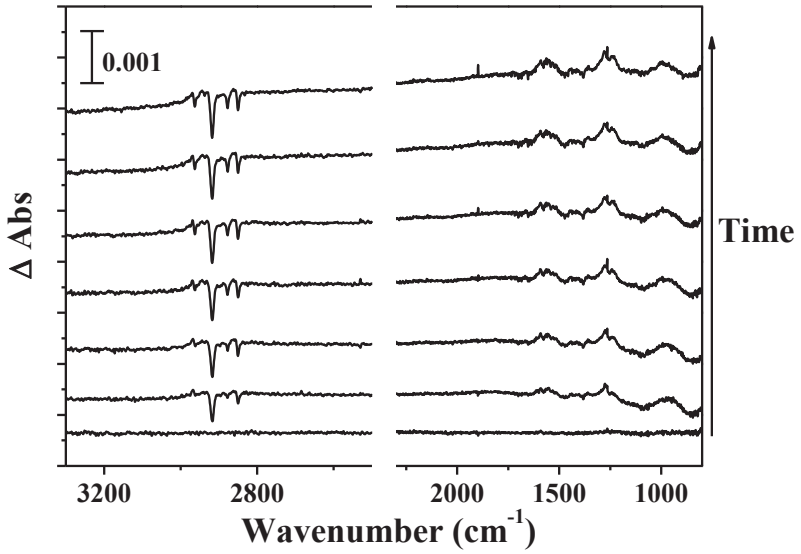

Figure 3.13. Reflection-absorption infrared difference spectra of an 18C methyl-termianted SAM during NO_3 exposure. The bottom spectrum is the monolayer with no exposure of NO_3, and the exposure increases by 2×10^3 L per spectrum from bottom to top with a total dose of 1×10^4 L of NO_3.

In Detoni and Paulson's IR studies on dialkyl and diaryl sulfates, they observed the absorption bands for the asymmetric O=S=O stretch at 1360-1420 cm^{-1} and the symmetric O=S=O stretch at 1195-1225 cm^{-1}.[69,70] No positive peaks are observed at these two regions, which suggests that the sulfur on the gold surface is not oxidized by nitrate radicals on the time scale of our measurements. We attribute this observation to the fact that there are fewer defects in the SAM with long hydrocarbon chains, because it has stronger Van de Waal interactions among methylenes to obtain a better packing.[71] Therefore, we speculate that the sulfur oxidation might happen at defects on the gold substrate. However, more evidence, such as XPS studies, is needed to support this speculation.

3.3.2.3 Monolayer Characterization after NO_3 Exposure

Figure 3.14 shows the reflection-absorption infrared spectrum of an 18-carbon (18C) methyl-terminated SAM on a polycrystalline gold substrate before and after 3 hours of exposure to NO_3. In this figure, the intensity is defined as $-\log(R/R_0)$ where R is the reflectance of the SAM and R_0 is the reflectance of a clean Au substrate. Several key features of the spectra are discussed below.

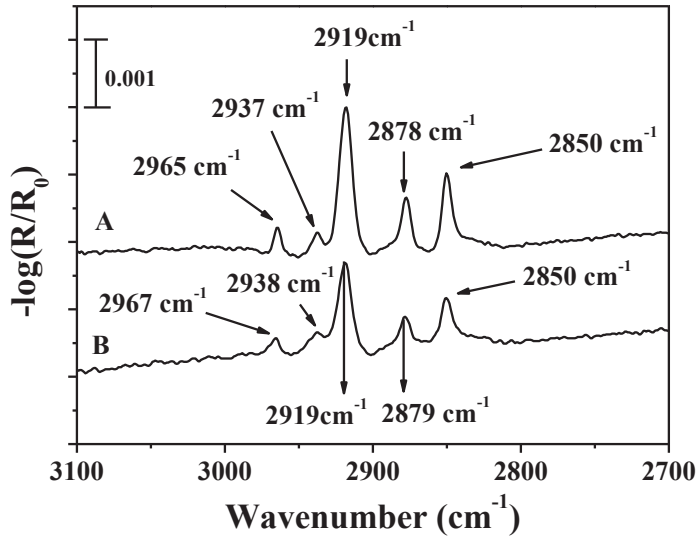

Figure 3.14. Reflection-absorption infrared spectra of an 18C methyl-terminated SAM before and after NO_3 exposure. The top spectrum (A) is the monolayer before exposure to NO_3 and the bottom spectrum (B) is the monolayer after 3 hours of NO_3 exposure.

After the surface was exposed to NO_3 for 3 hours, the peaks of the CH_2 stretch broadened, which might be caused by the disordering of the methylene chains. In addition, reactions between the monolayer and NO_3 would cause reorientation of the hydrocarbon chains. Because this reorientation could make the transition dipole moment of the CH_2 stretch less perpendicular to the surface than that before exposure, the peak intensities decreased. This decrease could also be due to chain desorption

from the surface. However, all peak intensities changed slightly, which indicated that only a small amount of the CH_2 groups was involved in the reaction and the reaction did not largely affect the orientation of the hydrocarbon chain. Therefore, even after 3 hours of NO_3 exposure, all four peaks were still observable.

3.3.2.4 Possible Pathways of NO_3 reaction with Methyl-terminated SAMs

Based on the data shown in Figures 3.10-3.14, we proposed the mechanism for reactions of NO_3 with methyl-terminated SAMs outlined in Figure 3.15. The mechanism illustrates that NO_3 can abstract a hydrogen atom from a methylene or a methyl to form the alkyl radical, which will react with NO_3 or NO_2 upon further exposure, generating organic nitrates or nitro compounds. Chain reorientation might take place during reactions of NO_3 with hydrocarbons. The IR data shows no oxidation of sulfur after 3 hours of NO_3 exposure to the surface, but no certain conclusion can be made because what would happen on the surface upon further exposure is still unknown. Therefore, shorter chain-length methyl SAM or longer exposure time experiments should be introduced to determine if there is oxidation of sulfur by NO_3. In addition, the generated alkyl radicals might undergo radical propagation until it is terminated by reaction with NO_3 or NO_2, or combination with a neighboring radical, or even chain desorption from the surface through radical propagation.

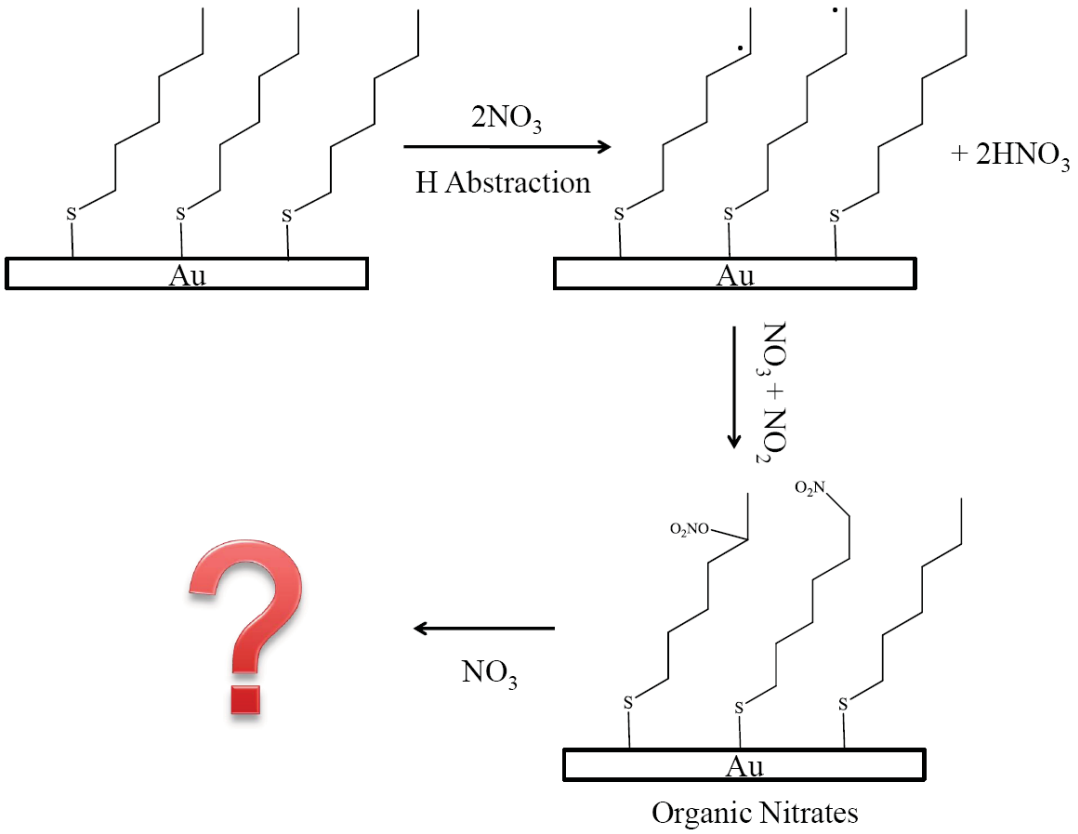

Figure 3.15. A proposed mechanism demonstrating the changes that occur during NO_3 reaction with methyl terminated self-assembled monolayers.

3.3.3 Summary

In summary, we monitored the heterogeneous oxidation of a vinyl- and a methyl-terminated self-assembled monolayer with NO_3 *in situ* with reflection-absorption infrared spectroscopy. The surface-bound products were monitored during the reaction. Using RAIRS, we were able to determine an observed rate constant for the reaction of an 18C vinyl terminated SAM with NO_3. The rate constant was used to calculate an initial reaction probability. The initial reaction probability was approximately two orders of magnitude higher than that for the reaction of the same SAM with O_3. The increased reaction probability can be explained when considering the difference in reactivity of ozone and NO_3 toward the

carbon-carbon double bonds. A mechanism for reactions between NO_3 and the vinyl-terminated SAM was proposed based on the kinetic data.

An 18C methyl-terminated SAM was characterized before and after NO_3 exposure with RAIRS. *In situ* studies of methyl-terminated SAM reaction with NO_3 suggested hydrogen abstraction from methylene or methyl groups by NO_3. On the time scale of our measurements, we observed no oxidation of sulfur in RAIRS. Further exploration with XPS needs to be done to confirm such conclusion. We proposed a mechanism for the reaction of NO_3 with the methyl-terminated SAM in which it stated that the SAM underwent hydrogen abstraction to form organic nitrates or nitro compounds.

Chapter 4

Summary and Future Research

4.1 Summary of Results

The main goal of my research is to investigate the fundamental chemistry of reaction kinetics, products, and mechanisms of NO_3 radicals with organic surfaces. Heterogeneous reactions between atmospheric NO_3 radicals and organic surfaces contribute significantly to the change in physical or chemical properties of organic aerosols. These changes can alter the particle's size, light absorption, and scattering. Therefore, exploring the reaction pathways will enable scientists to better predict the fate, lifetime, and environmental impact of organic aerosols in the atmosphere.

In an effort to develop an initial, very fundamental understanding of reactions between NO_3 radicals and organic surfaces, SAMs were used for these studies. The monolayers allow us to control the order, the chemical identity and the polarity of surfaces. An UHV system was used to perform experiments such as surface characterization and NO_3 exposure. A system was also developed to synthesize, store, and deliver NO_3 radicals to the surface analysis chamber. Reactions could be monitored *in situ* with RAIRS to identify products that were formed on the surface and to determine the reaction kinetics. Elemental analysis and oxidation state determination of surface-bound molecules before and after NO_3 exposure was realized with XPS. In addition, a mass spectrometer was employed to characterize the incident flux of NO_3 during an experiment.

To perform experiments mentioned above, we applied well-organized organic thin

films and monitored NO_3 reactions with the surfaces in the UHV system. An 18-carbon vinyl-terminated self-assembled monolayer was synthesized and the surface was characterized with RAIRS and XPS. The reaction of NO_3 radicals with the vinyl-terminated SAM was monitored *in situ* with RAIRS. The disappearance of carbon-carbon double bonds was observed concurrently with disordering of the methylene chains. XPS data showed the formation of organic nitrates and little oxidation of the sulfur head groups during the reaction. The oxidation kinetics of the vinyl groups was monitored using RAIRS. The observed rate constant was determined from the change in intensity of the absorption band of either the ν(C=C) stretch or the ν_s(-ONO_2) stretch. The observed rate constants that were calculated from both methods were consistent. This consistency indicated that the organic nitrate formed during the reaction was due to reactions of NO_3 radicals and the double bond. The rate constant was reported to be $(1.3 \pm 0.2) \times 10^{-3}$ s^{-1}. Based on this rate constant, an initial reaction probability was determined to be $(3 \pm 1) \times 10^{-3}$. The probability translates to three reactions occurring for every ~1000 collisions between gas-phase NO_3 radicals and the double bond at the interface. This reaction probability is approximately two orders of magnitude higher than when the same SAM is exposed to O_3.[65] The increase in the reaction probability is consistent with the increase in reactivity of NO_3 oxidation toward the double bond. A mechanism, which involved the double bond consumption and organic nitrate formation, was proposed.

To explore hydrogen abstraction during NO_3 exposure, an 18-carbon methyl-terminated SAM was synthesized. This methyl-terminated monolayer was

characterized before and after NO_3 exposure with RAIRS. Reactions between NO_3 radicals and the surface were monitored *in situ* using RAIRS. At the same time that the methylene groups disappeared, the formation of alkyl radicals and organic nitrates was observed. On the time scale of our measurements, no oxidation of sulfur head groups was observed in RAIRS. Further investigations using XPS are necessary to confirm this conclusion.

As a control for the reactions mentioned above, reactions of vinyl-terminated and methyl-terminated SAMs with pure NO/NO_2 were studied in the ultrahigh vacuum system. These studies are important because they help us to determine if NO/NO_2 molecules, which are produced upon NO_3 generation, play a role in the initial reaction rate of NO_3 radicals at the surface. For the NO and NO_2 studies, no changes to the RAIR spectra were observed above our signal-to-noise level after 30 min of exposure. This fact indicates that the initial reactivity of the SAMs toward NO/NO_2 was very low. However, our results suggest that NO_2 quickly adds to the alkyl radicals generated at the surface following the initial NO_3 addition to the vinyl group.

4.2 Future Research

Future work utilizing the UHV surface analysis chamber should include studies that monitor reactions while changing the surface temperature. These studies allow us to determine the reaction activation energy for further mechanism exploration. XPS experiments on reactions of NO_3 radicals with methyl-terminated SAMs should also be included. These experiments could identify oxidation states of surface-bound

molecules before and after NO_3 exposure. Future work should also include the detection of gas-phase products that were desorbed from surfaces to learn if there is chain desorption during NO_3 exposure. In addition, using SAMs with polar terminal groups, we can observe reactions between NO_3 radicals and polar surfaces or mixed surfaces. This will help us study how polarity affects reaction kinetics and mechanisms.

References

(1) Hallquist, M.; Wenger, J. C.; Baltensperger, U.; Rudich, Y.; Simpson, D.; Claeys, M.; Dommen, J.; Donahue, N. M.; George, C.; Goldstein, A. H.; Hamilton, J. F.; Herrmann, H.; Hoffmann, T.; Iinuma, Y.; Jang, M.; Jenkin, M. E.; Jimenez, J. L.; Kiendler-Scharr, A.; Maenhaut, W.; McFiggans, G. *Atmospheric Chemistry & Physics* **2009**, *9*, 5155-5236.

(2) Finlayson-Pitts, B. J.; Pitts, J. N. *Chemistry of the Upper and Lower Atmosphere: Theory, Experiments, and Applications*; Academic Press: San Diego, CA, 2000.

(3) Sze, N. D.; Ko, M. K. W. *Atmospheric Environment* **1980**, *14*, 1223-1239.

(4) Donaldson, K.; Li, X. Y.; MacNee, W. *Journal of Aerosol Science* **1998**, *29*, 553-560.

(5) Ellison, G. B.; Tuck, A. F.; Vaida, V. *J. Geophys. Res.* **1999**, *104*, 11633-11641.

(6) Novakov, T.; Corrigan, C. E.; Penner, J. E.; Chuang, C. C.; Rosario, O.; Bracero, O. L. M. *J. Geophys. Res.* **1997**, *102*, 21307-21313.

(7) Novakov, T.; Penner, J. E. *Nature* **1993**, *365*, 823-826.

(8) Okabe, H. *Photochemistry of Small Molecules*; Wiley: New York, 1978.

(9) Blacet, F. E. *Ind. Eng. Chem.* **1952**, *44*, 1339-1342.

(10) Vacha, R.; Cwiklik, L.; Rezac, J.; Hobza, P.; Jungwirth, P.; Valsaraj, K.; Bahr, S.; Kempter, V. *Journal of Physical Chemistry A* **2008**, *112*, 4942-4950.

(11) Waring, C.; King, K. L.; Bagot, P. A. J.; Costen, M. L.; Mckendrick, K. G. *Physical Chemistry Chemical Physics* **2011**, *13*, 8457-8469.

(12) Geyer, A.; Alicke, B.; Konrad, S.; Schmitz, T.; Stutz, J.; Platt, U. *Journal of Geophysical Research-Atmospheres* **2001**, *106*, 8013-8025.

(13) Platt, U.; Perner, D.; Winer, A. M.; Harris, G. W.; Pitts, J. N. *Geophysical Research Letters* **1980**, *7*, 89-92.

(14) Magnotta, F.; Johnston, H. S. *Geophys. Res. Lett.* **1980**, *7*, 769-772.

(15) Orlando, J. J.; Tyndall, G. S.; Moortgat, G. K.; Calvert, J. G. *The Journal of Physical Chemistry* **1993**, *97*, 10996-11000.

(16) Mentel, T. F.; Bleilebens, D.; Wahner, A. *Atmospheric Environment* **1996**, *30*, 4007-4020.

(17) Cantrell, C. A.; Davidson, J. A.; Busarow, K. L.; Calvert, J. G. *J. Geophys. Res.* **1986**, *91*, 5347-5353.

(18) Heintz, F.; Platt, U.; Flentje, H.; Dubois, R. *J. Geophys. Res.* **1996**, *101*, 22891-22910.

(19) Demore, W. B.; Margitan, J. J.; Molina, M. J.; Watson, R. T.; Golden, D. M.; Hampson, R. F.; Kurylo, M. J.; Howard, C. J.; Ravishankara, A. R. *International Journal of Chemical Kinetics* **1985**, *17*, 1135-1151.

(20) Noxon, J. F.; Norton, R. B.; Marovich, E. *Geophysical Research Letters* **1980**, *7*, 125-128.

(21) Asaf, D.; Tas, E.; Pedersen, D.; Peleg, M.; Luria, M. *Environ Sci Technol* **2010**, *44*, 5901-5907.

(22) Atkinson, R. *Atmospheric Environment Part a-General Topics* **1990**, *24*, 1-41.

(23) Winer, A. M.; Atkinson, R.; Pitts, J. N. *Science* **1984**, *224*, 156-159.

(24) Platt, U.; LeBras, G.; Poulet, G.; Burrows, J. P.; Moortgat, G. *Nature* **1990**, *348*,

147-149.
(25) Sandberg, J. S.; Basso, M. J.; Okin, B. A. *Science* **1978**, *200*, 1051-1054.
(26) Rasmussen, R. A. *J. Air Pollut. Control Assoc.* **1972**, *22*, 537-543.
(27) Skov, H.; Benter, T.; Schindler, R. N.; Hjorth, J.; Restelli, G. *Atmospheric Environment* **1994**, *28*, 1583-1592.
(28) Mellouki, A.; Lebras, G.; Poulet, G. *Journal of Physical Chemistry* **1988**, *92*, 2229-2234.
(29) Crowley, J. N.; Burrows, J. P.; Moortgat, G.; Poulet, G.; LeBras, G. *J. Chem. Kinet* **1990**, *22*, 673-681.
(30) Eberhard, J.; Howard, C. J. *The Journal of Chemical Physics A* **1997**, *101*, 3360-3366.
(31) Atkinson, R. *J. Phys. Chem. Ref. Data* **1997**, *26*, 215-290.
(32) Kaiser, E. W. *The Journal of Chemical Physics* **1995**, *99*, 707-711.
(33) Atkinson, R. *Atmospheric Environment* **2000**, *34*, 2063-2101.
(34) Atkinson, R.; Plum, C. N.; Carter, W. P. L.; Winer, A. M.; Pitts, J. N. *The Journal of Physical Chemistry* **1984**, *88*, 1210-1215.
(35) Aschmann, S. M.; Atkinson, R. *The Journal of Physical Chemistry A* **2011**, *115*, 1358-1363.
(36) Salgado, M.; Gallego-Iniesta, M.; Martín, M.; Tapia, A.; Cabañas, B. *Environmental Science and Pollution Research* **2011**, *18*, 940-948.
(37) Wang, K.; Ge, M. F.; Wang, W. G. *Chemical Physics Letters* **2010**, *490*, 29-33.
(38) Tapia, A.; Villanueva, F.; Salgado, M. S.; Cabañas, B.; Martínez, E.; Martín, P. *Atmospheric Chemistry & Physics* **2011**, *11*, 3227-3241.
(39) Goeschen, U. W. a. C. *Australian Journal of Chemistry* **2011**, *64*, 833-842.
(40) M. Ammann, U. P., Y. Rudich *Physical Chemistry Chemical Physics* **2003**, *5*, 351-356.
(41) Xiao, S.; Bertram, A. K. *Physical Chemistry Chemical Physics* **2011**, *13*, 6628-6636.
(42) Donaldson, D. J.; Mmereki, B. T.; Chaudhuri, S. R.; Handley, S.; Oh, M. *Faraday discussions of the Chemistry Society* **2005**, *130*, 227-239.
(43) Gross, S.; Bertram, A. K. *J. Geophys. Res.* **2009**, *114*, 1-14.
(44) Moise, T.; Talukdar, R. K.; Frost, G. J.; Fox, R. W.; Rudich, Y. *J. Geophys. Res.* **2002**, *107*, 1-6.
(45) Moise, T.; Rudich, Y. *Journal of Geophysical Research-Atmospheres* **2000**, *105*, 14667-14676.
(46) Nix, R. M. *Why is UHV required for surface studies?* 2003, <http://www.chem.qmul.ac.uk/surfaces/scc/scat4_2.htm>.
(47) Greenler, R. G. *The Journal of Chemical Physics* **1966**, *44*, 310-315.
(48) Peter Atkins, J. D. P. *Physical Chemistry*; Oxford University Press: New Delhi, 2007.
(49) Harris, D. C. *Quantitative Chemical Analysis*; Freeman: New York, 2007.
(50) Einstein, A. *Annalen der Physik* **1905**, *17*, 132-148.
(51) Briggs, D.; Seah, M. P. *Practical Surface Analysis by Auger and X-ray Photoelectron Spectroscopy*; John Wiley & Sons, 1983.
(52) Love, J. C.; Estroff, L. A.; Kriebel, J. K.; Nuzzo, R. G.; Whitesides, G. M. *Chemical*

Reviews **2005**, *105*, 1103-1170.
(53) Gates, B. D.; Xu, Q.; Stewart, M.; Ryan, D.; Willson, C. G.; Whitesides, G. M. *Chemical Reviews* **2005**, *105*, 1171-1196.
(54) Nuzzo, R. G.; Zegarski, B. R.; Dubois, L. H. *Journal of the American Chemical Society* **1987**, *109*, 733-740.
(55) Widrig, C. A.; Alves, C. A.; Porter, M. D. *Journal of the American Chemical Society* **1991**, *113*, 2805-2810.
(56) Ulman, A.; Eilers, J. E.; Tillman, N. *Langmuir* **1989**, *5*, 1147-1152.
(57) Dubois, L. H.; Nuzzo, R. G. *Annual Review of Physical Chemistry* **1992**, *43*, 437-463.
(58) Hu, J.; Fox, M. A. *Journal of Organic Chemistry* **1999**, *64*, 4959-4961.
(59) Duan, L.; Garrett, S. J. *Langmuir* **2001**, *17*, 2986-2994.
(60) Maroncelli, M.; Qi, S. P.; Strauss, H. L.; Snyder, R. G. *Journal of the American Chemical Society* **1982**, *104*, 6237-6247.
(61) Socrates, G. *Infrared and Raman Characteristic Group Frequencies: Tables and Charts*; 3 rd ed. ed.; John Wiley & Sons, Inc.: New York, 2001.
(62) Snyder, R. G.; Strauss, H. L.; Elliger, C. A. *Journal of Physical Chemistry* **1982**, *86*, 5145-5150.
(63) Atkinson, R. *Journal of physical and chemical reference data* **1991**, *20*, 459-507.
(64) Moore, J. H.; Davis, C. C.; Coplan, M. A. *Building Scientific Apparatus*; Cambridge University Press: Cambridge, 2009.
(65) Larry, R. F., Virginia Polytechnic Institute and State University, 2008.
(66) Wagner, A. J.; Carlo, S. R.; Vecitis, C. D.; Fairbrother, H. *Langmuir* **2002**, *18*, 1542-1549.
(67) Wagner, C. D.; Riggs, W. M.; Davis, L. E.; Moulder, J. F.; Muilenberg, G. E. *Handbook of X-ray Photoelectron Spectroscopy*; Perkin-Elmer Corporation, 1979.
(68) Allara, D. L.; Nuzzo, R. G. *Langmuir* **1985**, *1*, 52-66.
(69) Detoni, S.; Hadzi, D. *Spectrochim. Acta* **1957**, *17*, 601-608.
(70) Paulson, G.; Bakke, J.; Giddings, J.; Simpson, M. *Biological Mass Spectrometry* **1978**, *5*, 128-132.
(71) Vericat, C.; Vela, M. E.; Salvarezza, R. C. *Physical Chemistry Chemical Physics* **2005**, *7*, 3258-3268.